Biogeosciences, 21, 1477–1499, 2024
https://doi.org/10.5194/bg-21-1477-2024

Biogeosciences Open Access EGU

Distinct oxygenation modes of the Gulf of Oman over the past 43 000 years – a multi-proxy approach

Nicole Burdanowitz[1], Gerhard Schmiedl[1], Birgit Gaye[1], Philipp M. Munz[2], and Hartmut Schulz[2]

[1]Institute for Geology, Center for Earth System Research and Sustainability (CEN), Universität Hamburg, Bundesstraße 55, 20146 Hamburg, Germany
[2]Department of Geosciences, Eberhard Karls Universität Tübingen, Hölderlinstr. 12, 72074 Tübingen, Germany

Correspondence: Nicole Burdanowitz (nicole.burdanowitz@uni-hamburg.de)

Received: 9 November 2023 – Discussion started: 13 November 2023
Revised: 5 February 2024 – Accepted: 6 February 2024 – Published: 20 March 2024

Abstract. Changing climatic conditions can shape the strength and extent of the oxygen minimum zone (OMZ). The presence and variability of the OMZ in the Arabian Sea is of importance to the latter's ecosystem. The state of oxygenation has, for instance, an impact on the pelagic and benthic faunal community or the nitrogen and carbon cycles. It is important to understand the dynamics of the OMZ and related marine environmental conditions because of their climate feedbacks. In this study, we combined three independent proxies to reconstruct the oxygenation state of the water column and bottom water in the Gulf of Oman for the past 43 kyr approximately. This multi-proxy approach is done for the first time at the northeastern Oman margin located in the Gulf of Oman. We used bulk sedimentary nitrogen isotopes ($\delta^{15}N$) and the alkane ratio (lycopane $+n$-C_{35})/n-C_{31} and benthic foraminiferal faunal analysis to reconstruct the strength of the OMZ in the water column and bottom water oxygenation, respectively. Our results show that the Gulf of Oman experienced strong pronounced OMZ and bottom water deoxygenation during the Holocene. In contrast, during Marine Isotope Stage 2 (MIS 2), including the Last Glacial Maximum (LGM), the Gulf of Oman was very well ventilated, with a highly diverse benthic foraminiferal community. This may have been caused by stronger wind-induced mixing and better ventilation by oxygen-rich water masses. Our results also show moderate oxygenation during MIS 3, with deoxygenation events during most of the warmer Dansgaard–Oeschger (D–O) events. We propose two distinct oxygenation modes for the Gulf of Oman: (1) a stable period of either strongly pronounced water column OMZ and bottom water deoxygenation or well-oxygenated water column and bottom water conditions and (2) an unstable period of oscillating oxygenation states between moderately oxygenated (stadials) and deoxygenated (interstadials, D–O events) conditions. The unstable period may be triggered by an interstadial Atlantic meridional overturning circulation (AMOC) mode, which is required to initiate D–O events.

1 Introduction

Oxygen minimum zones (OMZs) are an important feature of the oceans. Although they cover only about 8 % of the total oceanic surface (Paulmier and Ruiz-Pino, 2009), they have a great impact on the marine environment and the carbon and nitrogen cycles (Friederich et al., 2008; Gruber, 2004; Paulmier et al., 2011; Rixen et al., 2020; Wakeham, 2020). For instance, denitrification plays a major role in the nitrogen cycle of OMZs, and denitrification also acts as the largest sink for nitrogen in the ocean (Gruber, 2004; Rixen et al., 2020). Moreover, OMZs have the potential to act as a source for greenhouse gases like N_2O, CO_2 or CH_4 (Friederich et al., 2008; Naqvi et al., 2010; Paulmier and Ruiz-Pino, 2009). Further, several studies show that the intensification and deoxygenation of OMZs are positively coupled to climate warming (e.g. Bopp et al., 2013; Breitburg et al., 2018; Busecke et al., 2022; Zhou et al., 2022). One of the strongest OMZs is located in the Arabian Sea, comprising about 17 % of the worldwide area of OMZs (Rixen et al., 2020). Over half of the permanently hypoxic shelf sediments are located in the northern Indian Ocean, affecting benthic ecosystems – for instance, the diversity of benthic foraminifera (Helly

and Levin, 2004; Levin, 2003). Although the diversity of benthic foraminifera is generally reduced under low-oxygen conditions, the OMZ faunas of the Arabian Sea seem to be more resilient to low-oxygen conditions when compared to other non-OMZ regions. This higher resilience can be attributed to a dominance of nitrate-respiring infaunal benthic foraminifera in OMZ regions (Schmiedl et al., 2023a).

The Gulf of Oman, as part of the Arabian Sea, is a complex and poorly understood region. It is influenced by the intrusion of warm, highly saline and more oxygenated Persian Gulf Water (PGW) when compared to the Arabian Sea Water. Different gyres in the Gulf of Oman and their seasonal variations lead to a patchy distribution of the PGW in this area (Pous et al., 2004; Wang et al., 2013). Little is known about the oceanic environmental conditions in the past and their response to climate change in this region as only a few sedimentary records and modelling studies exist (Cullen et al., 2000; Lachkar et al., 2019; Schmidt et al., 2020; Sirocko et al., 1991; Staubwasser et al., 2003). According to Lachkar et al. (2019), rising sea surface temperatures (SSTs) in the Persian Gulf, especially during the winter months, reduce the ability of the PGW to ventilate the upper OMZ in the Gulf of Oman due to shallower spreading of the PGW. The authors also concluded that a strengthening of the OMZ in the Gulf of Oman can be also induced by lower sea levels. In this scenario, the Persian Gulf has fallen dry, and, therefore, the ventilation via the PGW would stop completely (Lachkar et al., 2019). However, existing Holocene and late Pleistocene sedimentary records (cores M5/3a – 422 and Orgon4-KS8, Sirocko et al., 1991, 2000; Staubwasser et al., 2003) located below the OMZ in the Gulf of Oman do not investigate the oxygenation status in this area. Nevertheless, from sedimentary records in other parts of the Arabian Sea OMZ we know that the OMZ varied in its extend and volume in the past (Altabet et al., 2002; Böll et al., 2014; Burdanowitz et al., 2019; Gaye et al., 2018; Ivanochko et al., 2005; Möbius et al., 2011; Pichevin et al., 2007; Suthhof et al., 2001). Those records have shown a greater expansion of the OMZ during the Holocene (interstadial), also known as Marine Isotope Stage 1 (MIS 1), than during the Last Glacial Maximum (LGM, MIS 2) and stadials of MIS 3. Further, most of the rapid warming events of the Dansgaard–Oeschger (D–O) events during the last glacial period resulted in a strengthening of the OMZ, albeit each single D–O event had a different impact on a local scale (Altabet et al., 2002; Ivanochko et al., 2005; Pichevin et al., 2007). However, due to the lack of continuous high-resolution archives in the Gulf of Oman, little is known about the OMZ and bottom water oxygenation prior to the Holocene, especially without the influence of Persian Gulf water (PGW) in this area.

Most of the records are based on the qualitative reconstruction of the oxygenation status. The most commonly used proxy is the bulk δ^{15}N of marine sediments. The global average δ^{15}N of deep-water nitrate is about 4.8 ± 0.2 ‰, but in intermediate and surface water, the δ^{15}N of nitrate can deviate strongly from this value due to the isotopic fractionation associated with nitrogen-cycling processes (Sigman et al., 2000; Sigman and Fripiat, 2019). In oxygen-depleted environments, heterotrophic bacteria use nitrate as an electron acceptor to oxidize organic matter and reduce the nitrogen, in several steps, to nitrogen gas (Sigman and Fripiat, 2019). Denitrification is associated with a strong isotopic effect of 15 ‰–25 ‰ so that the residual nitrate becomes strongly enriched in ^{15}N and can thus have δ^{15}N values > 20 ‰ (Casciotti, 2016). Upward mixing and upwelling can transport this enriched isotopic signal where it is incorporated into phytoplankton. During the nitrate consumption, phytoplankton also use the lighter ^{14}N with an isotope discrimination factor of about 5 ‰ and incorporate the denitrification signal into the biomass (Montoya, 2008). After the biomass is deceased and sinks to the ocean floor, the denitrification signal is transported to the seafloor and can be stored in the sediments (e.g. Altabet et al., 1995; Gaye-Haake et al., 2005). Therefore, δ^{15}N values can be used as a proxy for the OMZ strength in the water column (e.g. Altabet et al., 1995; Reichart et al., 1997). However, diagenetic processes can alter sedimentary δ^{15}N values, especially under low sedimentation rates (Gaye-Haake et al., 2005; Jung et al., 1997; Junium et al., 2015; Möbius et al., 2011; Tesdal et al., 2013). Nevertheless, it was found that, in the Arabian Sea, especially under high sedimentation rates on the shelf and slope, sedimentary δ^{15}N values are a reliable indicator for past denitrification processes (Möbius et al., 2011).

Another rarely used biomarker is the isoprenoid hydrocarbon lycopane, which is mainly limited to sediments from OMZs or oceanic anoxic events in the past (van Bentum et al., 2009; Dummann et al., 2021; Farrington et al., 1988; Ogihara, 2014; Sabino et al., 2020, 2021; Sinninghe Damsté et al., 2003). It is discussed that photoautotrophic organisms probably produce lycopane, but its origin is not yet fully resolved (Freeman et al., 1994; Sinninghe Damsté et al., 2003; Wakeham et al., 1993). However, these studies have shown that lycopane is well preserved in anoxic environments and is degraded fast under oxic conditions. Lycopane often co-elutes with the *n*-alkane *n*-C_{35} (van Bentum et al., 2009; Naeher et al., 2012; Sabino et al., 2020; Sinninghe Damsté et al., 2003), with the latter mainly being produced by terrestrial plants (e.g. Eglinton and Hamilton, 1967; Meyers and Ishiwatari, 1993). Unusually high abundances of *n*-C_{35} and lycopane (if co-eluted) or lycopane alone were detected in some parts of the Arabian Sea, with the highest contents found within the OMZ (Schulte et al., 1999, 2000; Sinninghe Damsté et al., 2003). Therefore the (lycopane + *n*-C_{35})/*n*-C_{31} ratio can be used as an indicator for bottom water oxygenation, with ratios > 0.5 representing suboxic to anoxic conditions (van Bentum et al., 2009; Sinninghe Damsté et al., 2003). Whereas these two presented proxies are a qualitative way to reconstruct the OMZ strength and bottom water oxygenation, benthic foraminifera can be used to achieve a quantitative oxygenation status reconstruction. The different

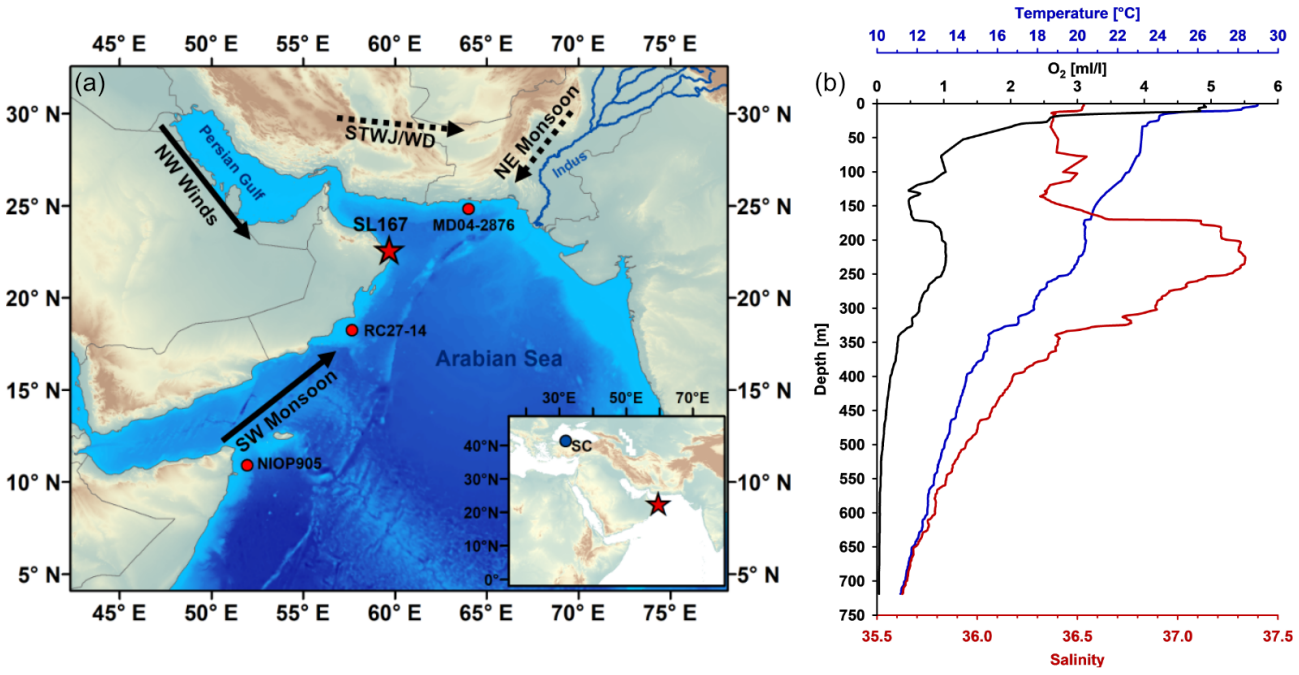

Figure 1. (a) Map of the study site SL167 (red star); nearby marine records (red circles) MD04-2876 (Pichevin et al., 2007), RC27-14 (Altabet et al., 2002) an NIOP905 (Ivanochko et al., 2005); and stalagmite record (blue circle in inset map) of Sofular Cave (SC) (Fleitmann et al., 2009). The black arrows (SW monsoon and NW winds) show the prevailing wind pattern during the summer, and the dashed black arrows (NE monsoon and subtropical westerly jet or western disturbances, STWJ/WD) indicate the prevailing wind pattern during the winter (after Clift and Plumb, 2008; Hunt et al., 2018). Map was created using ArcGIS v.10.8 (Esri, 2019). The bathymetric data are from the General Bathymetric Chart of the Oceans (GEBCO, 2014; http://www.gebco.net, last access: 4 January 2017). **(b)** Temperature (blue), oxygen (O_2, black) and salinity (red) depth profiles obtained at the end of the SW monsoon season in September 2007 during M74/1b cruise at the location of SL167.

benthic foraminifera species with their broad specific oxygen level requirements are widely used to reconstruct past bottom water oxygen conditions (e.g. Fontanier et al., 2002; Jorissen et al., 1995; Koho et al., 2008; Kranner et al., 2022; Lu et al., 2023; Schmiedl et al., 2000, 2010).

Here, we present the first high-resolution record reconstructing the OMZ strength and oxygen status of the bottom water at a depth situated within the present OMZ for the Holocene and late Pleistocene (past 43 kyr, approximately) at the Oman margin in the Gulf of Oman using a multi-proxy approach.

2 Modern oceanographic setting in the study area

The Gulf of Oman, as part of the northwestern Arabian Sea, connects the Arabian Sea via the Strait of Hormuz with the Persian Gulf. The northern Arabian Sea and the Gulf of Oman are affected by different water masses. At the surface, the Arabian Sea high-salinity water (ASHSW), with salinities between 35.3 and 36.7, comprises the upper 200 m (Kumar and Prasad, 1999; Shenoi et al., 1993). The highly saline (> 36.5) low-oxygen PGW is responsible for a weak ventilation of the upper OMZ (Fig. 1, 150–300 m water depth), especially in the southern part of the Gulf of Oman (Bower et al., 2000; Kumar and Prasad, 1999; Morrison et al., 1998; Pous et al., 2004; Prasad et al., 2001; Schmidt et al., 2020; Shenoi et al., 1993; Wang et al., 2013). The Red Sea Water (RSW, salinity: 35.1–35.6) enters the Arabian Sea via the Gulf of Aden and is found at intermediate water depths between 600 to 900 m (Bower et al., 2000; Kumar and Prasad, 1999). The RSW is transported northward along the Oman coast, especially during the SW monsoon (Acharya and Panigrahi, 2016; Beal et al., 2000; Kumar and Prasad, 1999; Schmidt et al., 2020). Another intermediate water mass (500–1000 m water depth) is the Indian Central Water (ICW), which is a mixture of the Antarctic Intermediate Water (AAIW) and the Indonesian Intermediate Water (IIW) and which enters the Arabian Sea during the SW monsoon via the Somali current along the Somali and Arabian coasts (Acharya and Panigrahi, 2016; Schott and McCreary, 2001). The initial oxygen-rich ICW becomes less oxygenated during its transport to the Arabian Sea (Acharya and Panigrahi, 2016). However, the oxygen content is still higher than that of the PGW and RSW (Rixen et al., 2014).

The region is influenced by different atmospheric circulations, which result in different seasonal primary-productivity patterns (Fig. 2). During the summer season, strong south-

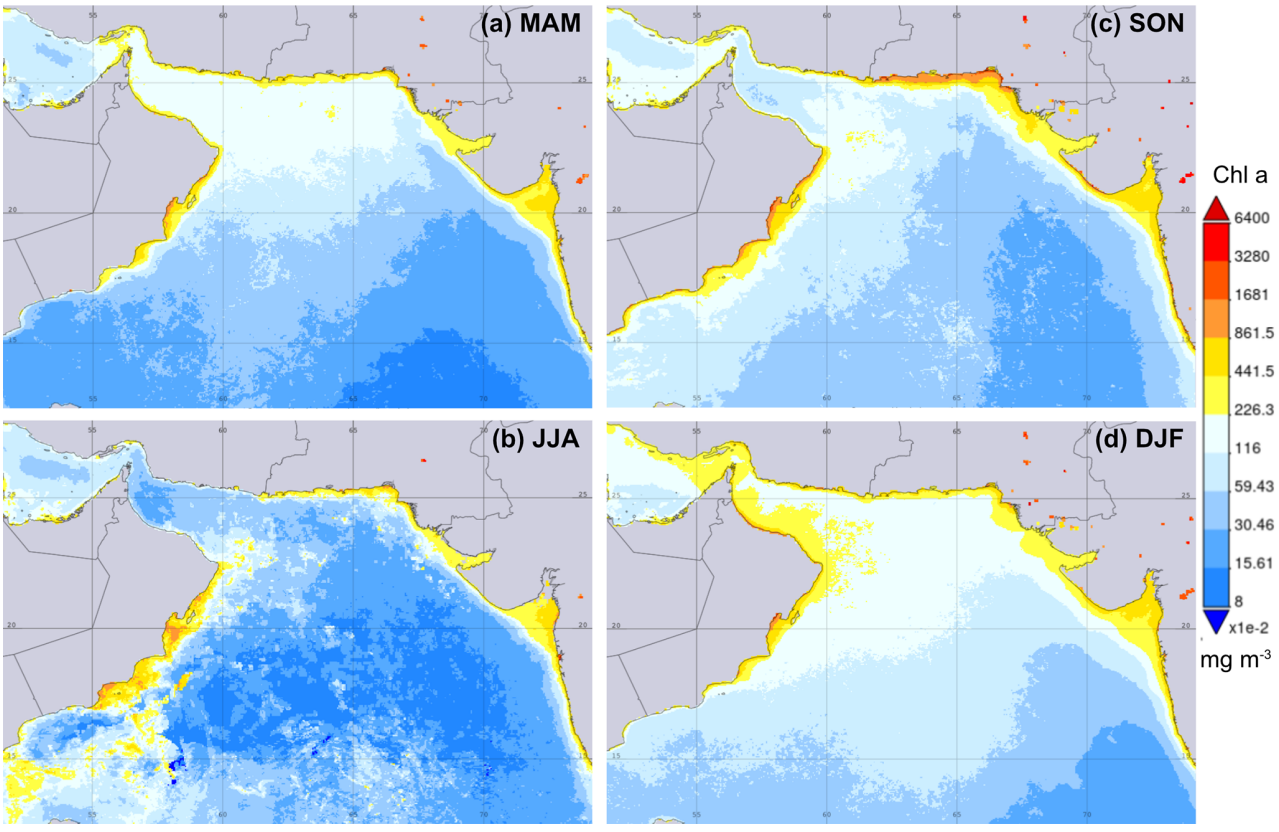

Figure 2. Average chlorophyll-*a* concentration (MODIS Aqua, L3m, 4 km spatial resolution, monthly) for the different seasons of **(a)** March–April–May (MAM), **(b)** June–July–August (JJA), **(c)** September–October–November (SON) and **(d)** December–January–February (DFJ) over the period from 2002 to 2022 (NASA, 2022). Data were visualized using the Giovanni online data system, developed and maintained by the NASA GES DISC (date of access: 26 January 2023).

west (SW) winds and the Findlater Jet in the western Arabian Sea induce upwelling and lateral transport of cold nutrient-rich water, resulting in high primary productivity (Fig. 2b) (Andruleit et al., 2003; Haake et al., 1993; Rixen et al., 2020). In contrast, the highest productivity in the northern Arabian Sea and Gulf of Oman is observed during the winter season (Fig. 2d) when high amounts of nutrients are available due to deeper wind-induced surface mixing by the NE winds (Böll et al., 2014; Madhupratap et al., 1996; Rixen et al., 2020). During the summer season, the Ras Al Hadd Jet in the northeastern corner of Oman can transport cold upwelled water into the Gulf of Oman via eddies (Schott and McCreary, 2001). Further, eddies generated in the Gulf of Oman transport PGW trapped in its core into the Arabian Sea (L'Hégaret et al., 2015; de Marez et al., 2019). Both may have an impact on the sea surface temperature, salinity and primary productivity in this region.

3 Material and methods

The 739 cm long gravity core SL167 was collected in the northwestern Arabian Sea from the northeastern Oman margin off northern Oman (Gulf of Oman – 22°37.15′ N, 59°41.49′ E; 774 m water depth) during the RV *Meteor* cruise M74/1b in 2007 (Fig. 1). In total, 371 samples were used for δ^{15}N analyses, with continuous sampling intervals of 2 cm. For lipid biomarker analyses, 225 samples were used, with an interval of 2 cm in the upper 162 cm of the core and, due to low total organic carbon content (unpublished), an interval of 4 cm below 162 cm. All sediment samples were freeze-dried and homogenized with an agate mortar and pestle prior to chemical treatment for the analyses. For the analyses of benthic foraminifera, 149 samples taken every 5 cm were used.

3.1 Dating and age model

The age model is based on 21 radiocarbon datings by accelerator mass spectrometry (AMS) measurements of surface-dwelling planktonic foraminifera, comprising *Globigerinoides* spp., *Globigerinella* spp. and *Orbulina universa*, at Beta Analytic Inc., Miami, USA. The age–depth model was developed by using the Bayesian model package BACON v.2.5.6 (Blaauw and Christen, 2011) within R statistical software (v.4.3, R Core Team, 2023). We used the default settings, except for accumulation mean (set to 50), memory

mean (set to 0.3) and the calibration curve (set to Marine20). We applied a deltaR (ΔR) of 93 ± 61 years. The ΔR is based on the weighted mean of two regional marine reservoir corrections (Muscat) by Southon et al. (2002) using the marine calibration database (Reimer and Reimer, 2001, http://calib.org/marine/, last access: 9 August 2021).

3.1.1 Lipid biomarker analyses

Total lipid extracts (TLEs) of about 3 to 18 g of the sediment samples were obtained by using a Dionex Accelerated Solvent Extractor (ASE 200) at 100 °C and 1000 PSI for 5 min (three cycles) using a solvent mixture of dichloromethane–methanol (DCM−−MeOH, 9 : 1) following the procedure described in Herrmann et al. (2016). Prior to extraction, a known amount of an internal standard (squalene) was added to the samples. After the extraction, TLEs were concentrated via rotary evaporation and transferred to combusted 4 mL vials. We have used $NaSO_4$ column chromatography to separate the TLEs into a hexane-soluble and hexane-insoluble fraction. Therefore, a combusted Pasteur pipette was packed with cleaned cotton wool and about 2 cm $NaSO_4$. The column was then first cleaned with about 8 mL hexane. Then, TLE was transferred with about 1 mL hexane to the column, and the remaining 4 mL vial was cleaned three times with about 1 mL hexane, which was also transferred to the column. For the hexane-insoluble fraction, about 1 mL of DCM was added four times to the column. The hexane-soluble fraction was saponified (85 °C, 2 h) in 5 % potassium hydroxide (KOH) in MeOH solution, and the neutral fraction was extracted with hexane. To obtain the *n*-alkane-containing apolar fraction from the neutral fraction, a column chromatography packed with deactivated silica gel (5 % H_2O, 60 mesh) was carried out by using hexane as a solvent. Afterwards, the apolar fraction was cleaned with hexane via column chromatography packed with silver-nitrate-coated silica gel ($AgNO_3$–Si).

For quantification of the *n*-alkanes, a Thermo Scientific TRACE 1310 gas chromatograph was coupled to a flame ionization detector (GC-FID) equipped with a Thermo Scientific TG-5MS column (30 m, 0.25 mm, 0.25 µm). The carrier gas H_2, with a flow rate of 35 mL min^{-1}, was used. The programmed temperature vaporizing (PTV) injector was operated starting at 50 °C, ramped by 10 °C s^{-1} to 325 °C in a splitless mode. The initial GC temperature was programmed to be 50 °C (held for 3 min) and was then increased by 6 °C min^{-1} to a final temperature of 325 °C, which was held for 20 min. For quantification of *n*-alkanes, an external standard containing the *n*-C_8–*n*-C_{40} alkanes was used at a known concentration. The quantification precision of repeated analyses of the external standard was 8 %.

The mass spectra of two samples (14–16 and 182–186 cm) were investigated with a Thermo Scientific TRACE GC Ultra coupled to a Thermo Scientific DSQ II mass spectrometer (GC-MS) with He (2 mL min^{-1} flow rate) as the carrier gas. The initial GC temperature of 50 °C was held for 3 min and ramped by 6 °C min^{-1} to 325 °C, with the final temperature being held for 25 min. To identify the compounds of the apolar fraction, the mass spectra were compared with published mass spectral data.

The average chain length (ACL) of plant-wax-derived *n*-alkanes is commonly used to identify plant functional types and environmental conditions (e.g. Collister et al., 1994; Cooper et al., 2015; Eglinton and Eglinton, 2008; Rommerskirchen et al., 2006). For instance, plants located in arid environments tend to have a longer ACL than plants in humid environments (e.g. Carr et al., 2014; Rommerskirchen et al., 2006; Vogts et al., 2009). But the ACL also differs with the plant functional type; for instance, C_4 grasses have, in general, a higher ACL than woody gymnosperms (e.g. Bush and McInerney, 2013; Carr et al., 2014; Cooper et al., 2015). However, the validity of the ACL is limited and, if possible, should be combined with compound-specific isotope measurements of the *n*-alkanes (e.g. Eglinton and Eglinton, 2008; Rommerskirchen et al., 2006; Vogts et al., 2009). We have calculated the ACL of *n*-alkanes using the following equation:

$$\mathrm{ACL}_{27\text{–}33} = \frac{27 \times \mathrm{C}_{27} + 29 \times \mathrm{C}_{29} + 31 \times \mathrm{C}_{31} + 33 \times \mathrm{C}_{33}}{\mathrm{C}_{27} + \mathrm{C}_{29} + \mathrm{C}_{31} + \mathrm{C}_{33}}. \quad (1)$$

The carbon preference index (CPI), an indicator of the odd-over-even predominance, is usable to distinguish between terrestrial plant and petroleum sources (e.g. Bray and Evans, 1961; Cranwell, 1978, 1981; Pancost and Boot, 2004). Terrestrial-plant-derived *n*-alkanes and recent sediments with unaltered organic material have an odd-over-even predominance, with a CPI higher than 3 (e.g. Bray and Evans, 1961). In contrast, petroleum sources have higher abundance of even *n*-alkanes, with CPIs < 1, and are an indication of higher degradation (e.g. Bray and Evans, 1961). The CPI was calculated by using the following equation:

$$\mathrm{CPI}_{27\text{–}33} = 0.5 \times \left(\frac{\mathrm{C}_{27} + \mathrm{C}_{29} + \mathrm{C}_{31} + \mathrm{C}_{33}}{\mathrm{C}_{26} + \mathrm{C}_{28} + \mathrm{C}_{30} + \mathrm{C}_{32}} + \frac{\mathrm{C}_{27} + \mathrm{C}_{29} + \mathrm{C}_{31} + \mathrm{C}_{33}}{\mathrm{C}_{28} + \mathrm{C}_{30} + \mathrm{C}_{32} + \mathrm{C}_{34}} \right), \quad (2)$$

where C_x is the concentration of the *n*-alkane with *x* atoms.

3.2 Bulk nitrogen isotope (δ^{15}N) analyses

For the δ^{15}N analyses, following the procedure described in Menzel et al. (2014), 6 to 61 mg of the freeze-dried and homogenized sediment was weighted into Sn capsules. δ^{15}N values were obtained by combusting the samples at 1050 °C in a Thermo Scientific Flash EA 1112 elemental analyser coupled to a Finnigan MAT 252 isotope ratio mass spectrometer. Nitrogen was calibrated against the International Atomic Energy Agency (IAEA) reference standards IAEA-1 and IAEA-2. In addition to being internal standards, both

(IAEA-1 and IAEA-2) were used as working standards. Replicate measurements of these standards yielded a precision better than 0.2 ‰. The samples were measured in duplicate, with a mean standard deviation of 0.07 ‰.

3.3 Benthic foraminifera analyses

For faunal analyses, between 198 and 558 (average of 311) individuals were at each depth, counted from representative splits of the size fraction > 125 µm. Species assignment is mainly based on Jones (1994), Den Dulk (2000), Szarek (2001), Schumacher et al. (2007) and Debenay (2012). Allochthonous shelf taxa, including larger benthic foraminifera (e.g. genera *Amphistegina*, *Heterostegina*, *Borelis*, *Peneroplis*), typical neritic taxa (e.g. *Ammonia* spp., *Cibicides refulgens*, *Elphidium* spp., *Lobatula lobatula*) and taxa with floating chambers (genera *Cymbaloporetta*, *Millettiana*, *Tretomphalus*, *Tretomphaloides*), were removed from the census data set (Murray, 1991). For benthic foraminiferal diversity, the Shannon Index H(S) was calculated according to Buzas and Gibson (1969). The H(S) considers the number of species and their relative proportion in the sample. The H(S) value is at a maximum when all species have equal proportions, while species with low abundances contribute little to it. In eutrophic to mesotrophic ecosystems, the diversity and microhabitat structure are oxygen controlled, as predicted by the TROX (trophic-oxygen) model (Gooday, 2003; Jorissen et al., 1995) (Fig. 3). For the estimation of bottom water oxygenation, the different taxa were classified into oxic, suboxic and dysoxic taxa based on their modern microhabitat preferences (Table S1 in the Supplement) (Schmiedl et al., 2023a). Bottom water oxygen concentrations were then calculated based on the enhanced benthic foraminiferal oxygen index and associated transfer function of Kranner et al. (2022), with the modification of Schmiedl et al. (2023a). The mean standard deviation (SD) across the entire oxygen range (0–6 $mL\,L^{-1}$) is $\pm 0.61\,mL\,L^{-1}$. However, the SD is lower in suboxic to dysoxic conditions, with SDs of ± 0.49 and $\pm 0.08\,mL\,L^{-1}$ across oxygen ranges of 1–2 and 0–1 $mL\,L^{-1}$, respectively. The expected relation between oxygen concentration and benthic foraminiferal diversity is clearly expressed at core site SL167 since it is influenced by comparatively high organic matter fluxes and low-oxygen conditions (Fig. 3).

3.4 Statistics

To identify periodicities in our data sets we performed spectral and wavelet analyses in R (v.4.3, R Core Team, 2023). For the spectral analysis, we used the REDFIT function of the package dplR v.1.7.4 (Bunn et al., 2022; Bunn, 2008, 2010), which is based on the Fortran 90 REDFIT source code by Schulz and Mudelsee (2002). For the wavelet analysis the data sets were first interpolated to an evenly spaced data set by using the package ncdf4.helpers v.0.3-6 (Bronough, 2021) and the approx. function. The wavelet analyses were performed with the package biwavelet v.0.20.21 (Gouhier et al., 2021) using the Morlet wavelet function and bias-corrected power spectrum, which is based on Torrence and Compo (1998).

4 Results

4.1 Age model of SL167

The results of the AMS radiocarbon measurements are shown in Table 1. The core SL167 comprises the last 42.6 kyr, approximately (Fig. 4). However, the last 3 kyr are missing in the core as the core top represents ca. 3.1 ka. The mean sedimentation rates range between 0.10 and 0.49 $mm\,yr^{-1}$, with higher sedimentation rates during the Holocene compared to the Pleistocene.

4.2 Lipid biomarker and δ^{15}N reconstructions

The samples of SL167 show a strong odd-over-even carbon number predominance with CPI values ranging between 2 and 13.8, and they show a dominance of land-plant-derived long-chain *n*-alkanes, where the $ACL_{27–33}$ varies between 30 and 31.2 (Fig. A1 in the Appendix). In some samples, for land-plant-derived *n*-alkanes, unusually high contents of the *n*-alkane C_{35} were detected in the GC-FID chromatograms. We chose one exemplary sample with a very high content of *n*-C_{35} and one sample with an usual distribution of land-plant-derived *n*-alkanes for mass spectral analyses. For the latter one, we found only the mass spectra of the *n*-alkane C_{35} at the expected retention time. However, for the sample with the high *n*-C_{35} content and unusual *n*-alkane distribution pattern, we found the mass spectra of both lycopane (2,6,10,14,19,23,27,31-octamethyldotriacontane) and *n*-C_{35} (Fig. 5). The characteristic fragments of lycopane are the ions of m/z 113, 183, 253, 309, 337, 407 and 447 (Sinninghe Damsté et al., 2003), which are also detected in our sample with the co-elution of *n*-C_{35} and lycopane (Fig. 5b). It is known from other studies that *n*-C_{35} and lycopane can co-elute during gas chromatography measurements (van Bentum et al., 2009; Sabino et al., 2020; Sinninghe Damsté et al., 2003).

The (lycopane + *n*-C_{35})/*n*-C_{31} varies between 0.1 and 1.7 throughout the core (Fig. 6d). The highest ratios occur during the late Holocene (3–4 ka) and warmer Pleistocene periods reconstructed from the NGRIP ice core δ^{18}O (North Greenland Ice Core Project members, 2004) and Sofular Cave δ^{13}C records (Fleitmann et al., 2009), respectively.

The δ^{15}N values in our Gulf of Oman record vary between 4.7 and 9.2 ‰ (Fig. 6b), with constantly high values throughout the Holocene (> 7.2 ‰). The variability of δ^{15}N is high (4.5 ‰) during the Pleistocene, with higher values > 7 ‰ during warmer phases.

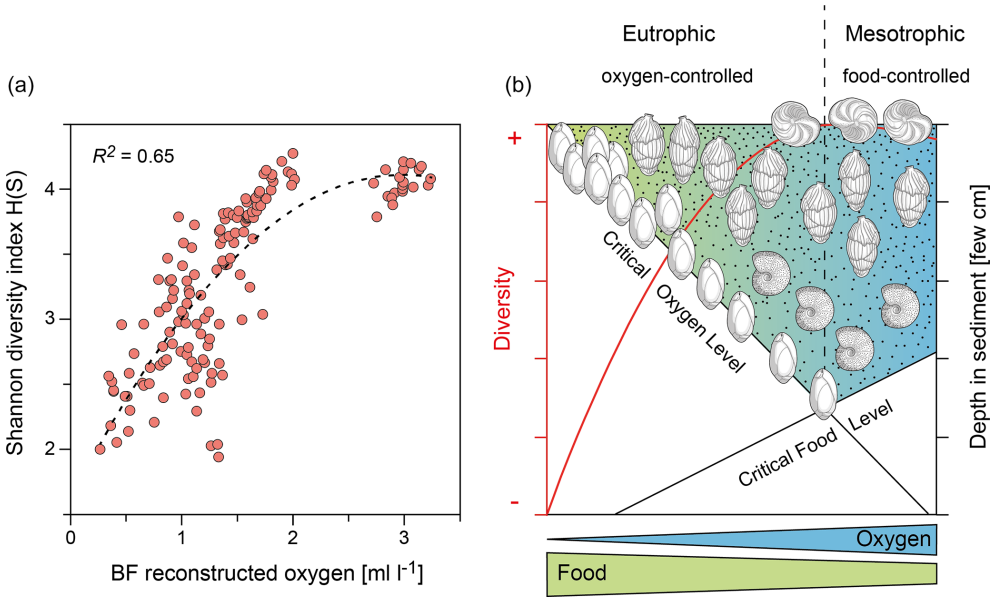

Figure 3. **(a)** Eutrophic to mesotrophic section of the trophic-oxygen (TROX) model of Jorissen et al. (1995), with the addition of Gooday (2003) describing the general dependence of benthic foraminiferal microhabitat structure and diversity from oxygen concentration and food supply. Figure modified from Schmiedl et al. (2023a). **(b)** Reconstructed dissolved oxygen concentration of bottom and pore waters versus benthic foraminiferal diversity H(S) for core SL167. The stippled line represents a polynomial of the second-degree model with $p < 0.001$. The observed significant correlation suggests a dominant oxygen control of benthic foraminiferal diversity at site SL167.

Table 1. AMS ^{14}C dates of planktic foraminifera of sediment core SL167 and calibrated ages using Calib 8.2 with Marine20 calibration curve and ΔR of 93 ± 61 years.

Depth interval (cm)	Mean depth (cm)	Material	^{14}C age (yr BP)	Calendar age 95.4 % prob. (yr BP)	Calendar age max (yr BP)	Calendar age min (yr BP)
4.5–5.5	5	Planktic foraminifera	3790 ± 30	3457 ± 216	3673	3241
19.5–20.5	20	Planktic foraminifera	3910 ± 30	3604 ± 217	3821	3387
40–41	40.5	Planktic foraminifera	4280 ± 30	4083 ± 241	4323	3842
59.5–60.5	60	Planktic foraminifera	6000 ± 30	6112 ± 194	6305	5918
79.5–80.5	80	Planktic foraminifera	5350 ± 30	5425 ± 193	5618	5232
119.5–120.5	120	Planktic foraminifera	7000 ± 30	7216 ± 196	7412	7020
140–141	140.5	Planktic foraminifera	7230 ± 30	7432 ± 171	7602	7261
160–161	160.5	Planktic foraminifera	8160 ± 30	8364 ± 192	8556	8172
179–181	180	Planktic foraminifera	9200 ± 30	9673 ± 225	9897	9448
220–221	220.5	Planktic foraminifera	9010 ± 30	9410 ± 202	9612	9208
239.5–240.5	240	Planktic foraminifera	11 300 ± 30	12 576 ± 176	12 737	12 386
259–261	260	Planktic foraminifera	11 170 ± 30	12 413 ± 241	12 654	12 172
299–302	300.5	Planktic foraminifera	13 080 ± 40	14 679 ± 345	15 024	14 334
340.5–341.5	341	Planktic foraminifera	13 980 ± 40	15 936 ± 284	16 219	15 652
399–401	400	Planktic foraminifera	19 200 ± 70	22 178 ± 263	22 441	21 915
460–461	460.5	Planktic foraminifera	18 430 ± 50	21 260 ± 350	21 609	20 910
510–511	510.5	Planktic foraminifera	26 950 ± 120	30 252 ± 338	30 590	29 914
559.5–560.5	560	Planktic foraminifera	29 260 ± 140	32 593 ± 539	33 132	32 054
599–601	600	Planktic foraminifera	33 930 ± 230	37 818 ± 777	38 595	37 041
660–661	660.5	Planktic foraminifera	34 260 ± 220	38 255 ± 720	38 974	37 535
720–722	721	Planktic foraminifera	38 290 ± 320	41 684 ± 415	42 098	41 269

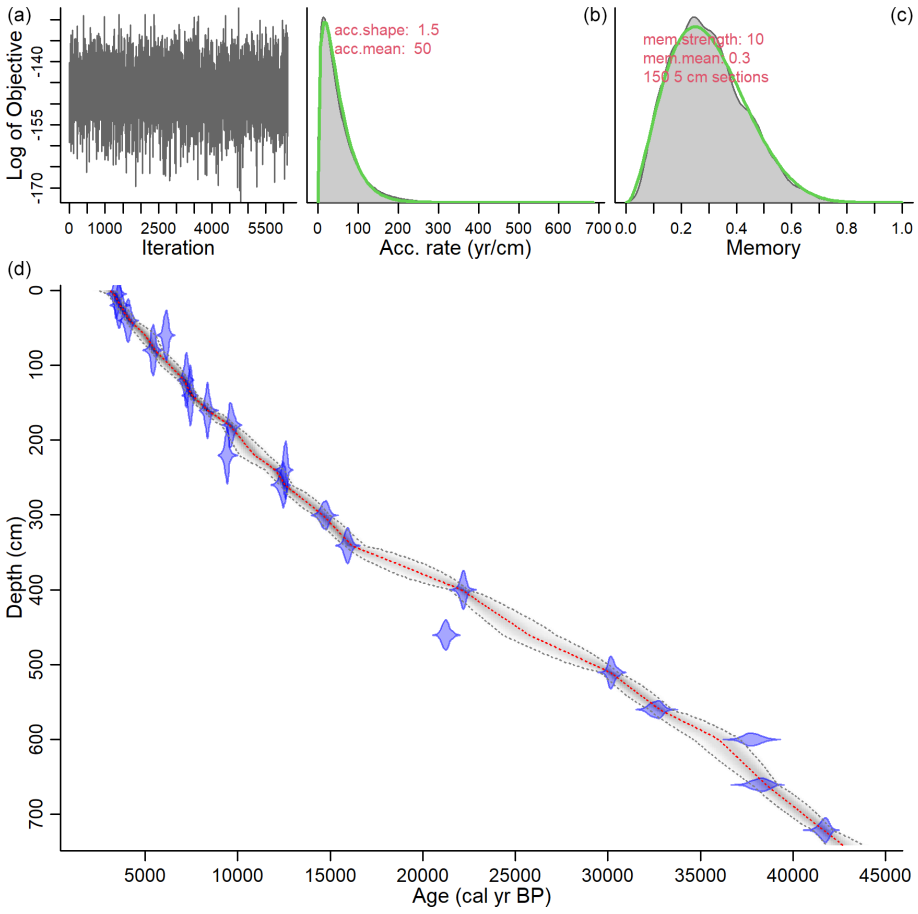

Figure 4. Age–depth model of SL167 using the R package BACON v. 2.5.6 (Blaauw and Christen, 2011). The upper panels **(a–c)** show the Markov chain Monte Carlo iterations **(a)**, the distributions of the prior (green curve) and posterior (grey area) accumulation rates **(b)**, and memory **(c)**. The lower panel **(d)** shows the age–depth model of SL167. The calibrated ^{14}C dates are shown in blue. The red line shows the modelled mean age of SL167 with the 95 % confidence interval (dotted black lines). A ΔR of 93 ± 61 years was applied.

4.3 Benthic foraminiferal diversity and reconstructed bottom water oxygenation

Overall, the benthic foraminiferal diversity is high and ranges between H(S) = 1.94 and 4.27 (average of 3.31 ± 0.64 SD). Significant fluctuations occur in the older part of the core, with minima during interstadials, while Heinrich events H2 and H1 and the Last Glacial Maximum are characterized by comparatively high H(S) values (Fig. 6). During the Holocene, the H(S) values exhibit a gradual decrease. The reconstructed oxygen values range between 0.27 and 3.25 (average of 1.46 ± 0.74 SD) and are negatively correlated to the benthic foraminiferal diversity and δ^{15}N. D–O and B–A events and the Holocene are characterized by relatively low oxygen concentrations, while cold intervals, particularly the interval around H1, exhibit higher values (Fig. 6).

5 Discussion

The δ^{15}N is often used as an indicator for past denitrification processes and, in the Arabian Sea, the strength of the OMZ (e.g. Altabet et al., 2002; Gaye et al., 2018; Ivanochko et al., 2005; Möbius et al., 2011; Pichevin et al., 2007). However, the δ^{15}N signal can be biased by different processes, which need to be considered. One factor is a diagenetic overprint of δ^{15}N leading to an enrichment of the heavier ^{15}N isotope, especially under low sedimentation rates (3–4 cm kyr^{-1}) (Altabet et al., 1999; Gaye-Haake et al., 2005; Jung et al., 1997; Junium et al., 2015; Möbius et al., 2011; Tesdal et al., 2013). In contrast, shelf and slope sediments deposited under high sedimentation rates in the Arabian Sea are considered to have unaltered δ^{15}N values and, therefore, are considered to be a reliable indicator for past denitrification processes (Möbius et al., 2011). The sedimentation rates are high in SL167 and vary between 9.7 and 49 cm kyr^{-1}. Further, they correlate with the nitrogen content but not with δ^{15}N values (Fig. A2). The correlation of the nitrogen content and δ^{15}N may due

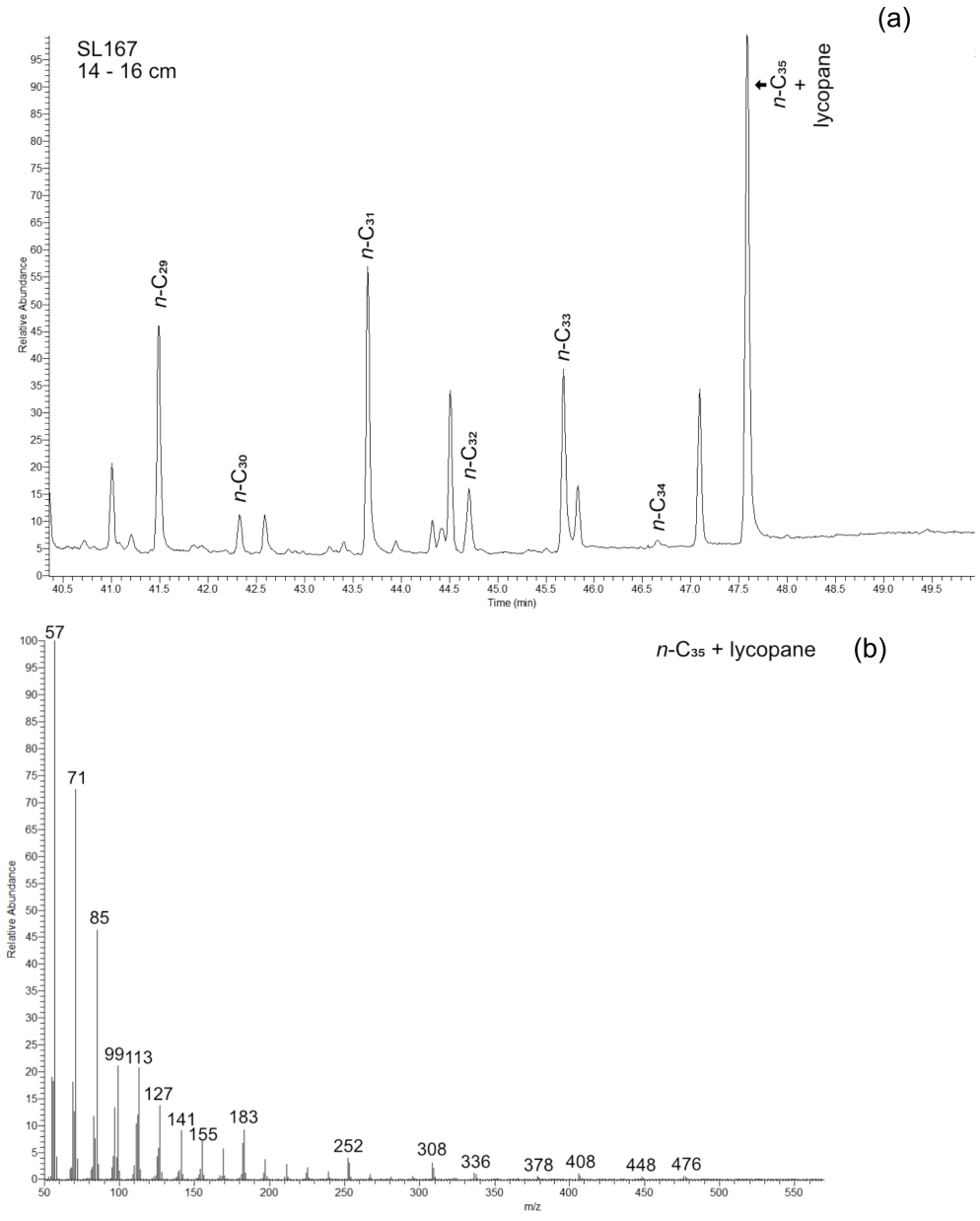

Figure 5. GC-MS measurement of the apolar fraction of sample from 14 to 16 cm sediment depth with retention time **(a)** and mass spectra of the *n*-alkane C_{35} + lycopane **(b)**.

to higher productivity and/or better preservation of organic matter under sub-anoxic conditions. Therefore, we argue that sedimentary $\delta^{15}N$ values in SL167 are a reliable indicator for past denitrification processes. However, it may be possible that the $\delta^{15}N$ signal in SL 167 is affected by changes in the water mass transport, mixing or lateral transport from e.g. the Oman upwelling area.

5.1 Strength of the OMZ and bottom water oxygenation in the Gulf of Oman

5.1.1 Pleistocene

Both independent proxies for bottom water oxygenation – (lycopane + *n*-C_{35})/*n*-C_{31} ratio and the O_2 reconstruction by benthic foraminifera – and the Shannon diversity index are in very good agreement, at least for the Pleistocene part of the core (Fig. 6a, c and d). Phases of sub-anoxic bottom water match well with observed interstadials, the D–O events, in the Greenland ice core records, e.g. NGRIP (North Green-

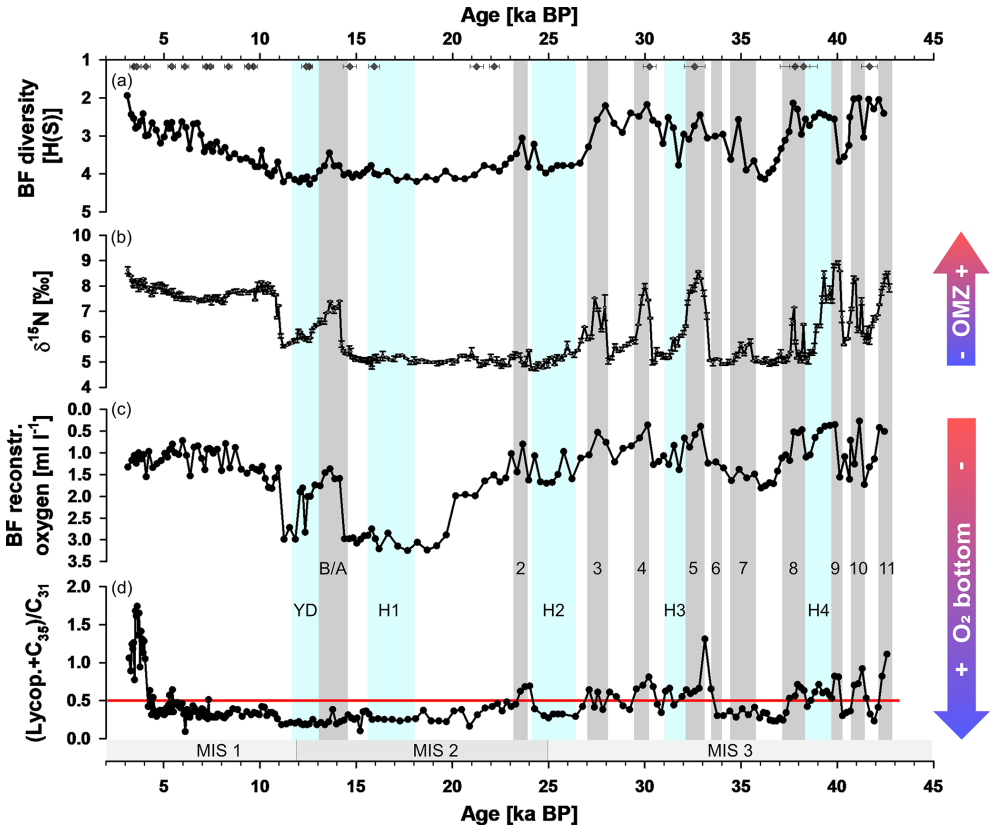

Figure 6. Oxygen proxies of SL167. Shannon Wiener (H(S)) diversity index for benthic foraminifera (BF) **(a)**, nitrogen isotope values (δ^{15}N) as denitrification and oxygen minimum zone (OMZ) strength indicator for the water column **(b)**, reconstructed bottom water oxygen content by benthic foraminifera **(c)**, and ratio of (lycopane $+n$-C_{35})/n-C_{31} as indicator for bottom water oxygen **(d)**. The red line in panel **(d)** indicates the threshold of oxic to suboxic to anoxic conditions (Sinninghe Damsté et al., 2003). Grey bars indicate Bølling–Allerød (B–A) and Dansgaard–Oeschger events (D–O, numbers), mostly based on Fleitmann et al. (2009). Blue bars indicate Younger Dryas event based on Fleitmann et al. (2009) and Heinrich (H) events based on a compilation by Allard et al. (2021). Diamonds show dated ages of SL167. Note the reversed axes for H(S) and BF reconstructed oxygen. The grey bars at the bottom represent the different Marine Isotope Stages (MISs).

land Ice Core Project members, 2004), except for D–O 6 and 7. The highest reconstructed bottom water oxygen content (up to 3.2 mL L^{-1}) occurred from about 14.3 to 19.6 ka and during the Younger Dryas between 11.2 and 12.3 ka (Fig. 6c). Further, MIS 3 (about 25–43 ka), is characterized by several distinct peaks of a strong OMZ (Fig. 6b) in the water column. Note that we used the Sofular Cave δ^{13}C record from Turkey (Fleitmann et al., 2009) instead of the NGRIP to allocate the distinct D–O events as this seems to be more appropriate (Fig. 7). Fleitmann et al. (2009) found a systematic age offset for most D–O events between the NGRIP and the more regional Sofular and Hulu cave (China) records of several centennial years, with younger ages for the D–O events in the NGRIP record. The D–O events 3–5 and 8–11 are well pronounced as strong abrupt OMZ intervals in the Gulf of Oman. In contrast, in the nearby Oman upwelling (core RC27-14), all D–O events, except 11, are expressed as strong OMZ intervals in the water column (Fig. 7c) (Altabet et al., 2002). A high-resolution record (MD04-2876) in the northern Arabian Sea shows a similar pattern as core RC27-14 (Pichevin et al., 2007), whereas a record (NIOP905) from the more southern Somali upwelling area (Ivanochko et al., 2005) does not show a strong OMZ in the water column during the first four D–O events (Fig. 7b and d). Note that shifts in OMZ peaks of the different records in the Arabian Sea may be due to age uncertainty, as well as peak tuning of the other records with the Greenland ice core (GISP2) δ^{18}O record.

Bottom water oxygenation may be driven not only by processes in the upper water column but also by the occurrence of different water masses. The RSW is transported northward, especially during the SW monsoon (Acharya and Panigrahi, 2016; Beal et al., 2000; Kumar and Prasad, 1999), and may undergo oxygen depletion due to higher organic matter supply and its decay on its way to the Gulf of Oman (Pathak et al., 2021). Acharya and Panigrahi (2016) have shown that today's RSW core extends between 600 and 660 m, nearly reaching the seafloor at the core site (∼ 740 m). Thus, phases with stronger SW monsoons, such as the D–O interstadials, are characterized by more inputs of low-oxygen RSW and, therefore, sub-anoxic conditions of bottom water in the

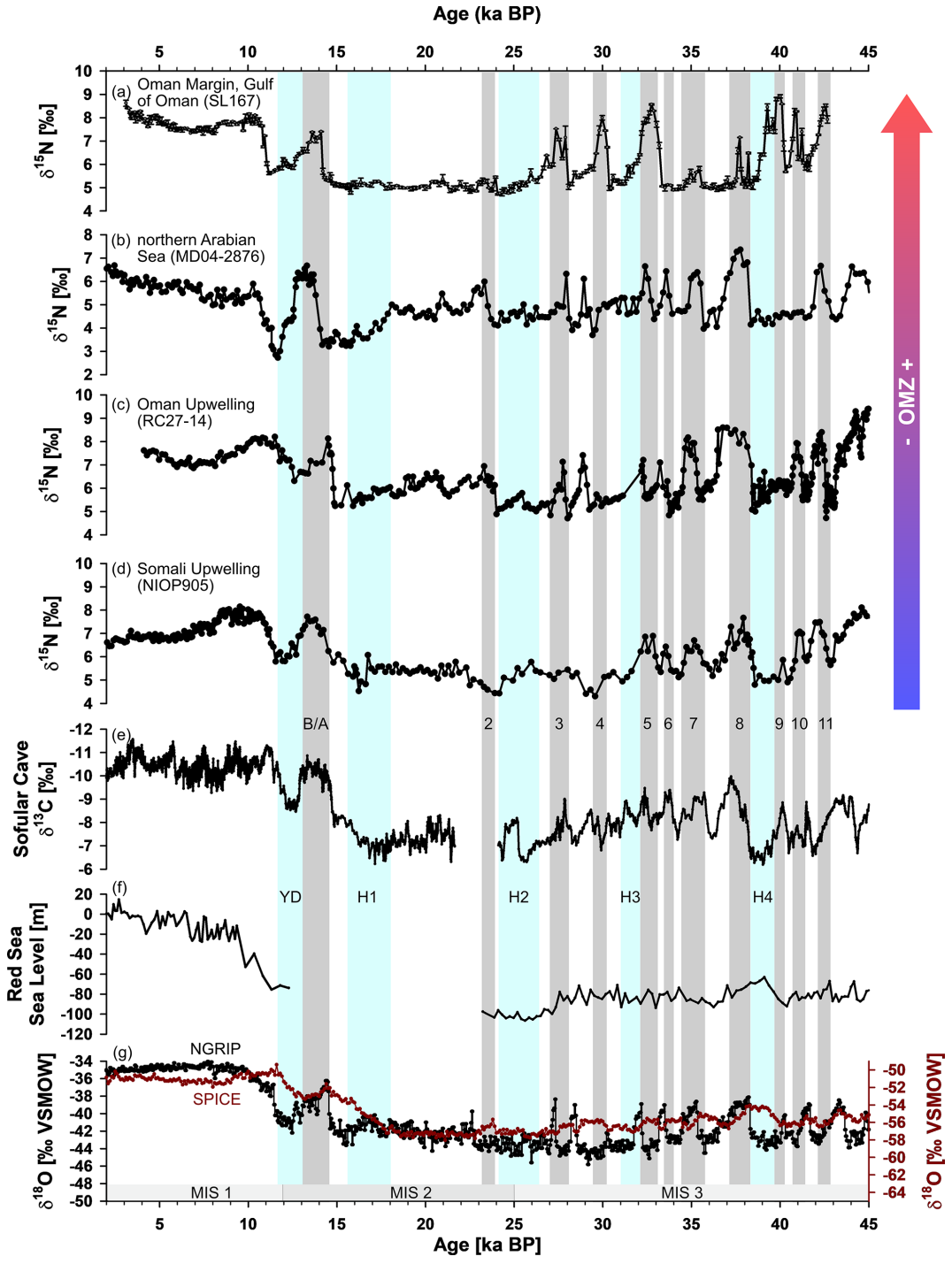

Figure 7. Comparison of high-resolution nitrogen isotope (δ^{15}N) records in the Arabian Sea. SL167 (this study) from the Gulf of Oman **(a)**, MD04-2876 (Pichevin et al., 2007) from the Pakistan margin in the northern Arabian Sea **(b)**, RC27-14 (Altabet et al., 2002) from the Oman upwelling region in the western Arabian Sea **(c)** and NIOP905 (Ivanochko et al., 2005) from the Somali upwelling in the southwestern Arabian Sea **(d)**. Grey bars indicate Bølling–Allerød (B–A) and Dansgaard–Oeschger events (D–O, numbers), mostly based on the δ^{13}C Sofular Cave record **(e)** by Fleitmann et al. (2009). Combined Red Sea sea level reconstruction of sediment core KL11 **(f)** by Siddall et al. (2003) and Rohling et al. (2008) for the Holocene and Pleistocene, respectively. The δ^{18}O records of NGRIP (North Greenland Ice Core Project members, 2004) and SPICE (Steig et al., 2021) are shown in **(g)**. Blue bars indicate Younger Dryas event based on Fleitmann et al. (2009) and Heinrich (H) events based on a compilation by Allard et al. (2021). The grey bars at the bottom represent the different Marine Isotope Stages (MISs).

Gulf of Oman. This corroborates findings from the Oman upwelling area, where oxygen bottom water reconstructions using benthic foraminifera show oxygen-depleted conditions during phases with higher outflows of RSW into the northwestern Arabian Sea (Pathak et al., 2021).

The missing D–O 6 and weak D–O 7 events might be a result of the combination of local or regional and global conditions. First, the strength of the Indian and Asian monsoon systems are strongly coupled to high-latitude climate (e.g. Deplazes et al., 2013, 2014; Overpeck et al., 1996; Schulz et al., 1998; Singh et al., 2011; Wang et al., 2001). Phases with strong monsoon intervals are coupled to the D–O events found in Greenland ice cores. However, the duration and strength of both varied through the time. In some records from the Asian region, D–O 6 had a weaker environmental impact than other D–O events (e.g. Deplazes et al., 2014; Ivanochko et al., 2005; Wang et al., 2001). Second, the fluctuation of the Red Sea sea level (Fig. 7f) could lead to variations in the exchange of the RSW and the Indian Ocean or Arabian Sea, with a stronger influence during higher sea levels and vice versa (Arz et al., 2007; Siddall et al., 2003). However, the sea level was, in general, lower during MIS 3 than during the Holocene, which might have led to a weaker influence of the RSW compared to recent conditions (Rohling et al., 2008; Siddall et al., 2003). Third, the degree of northward extension of the oxygen-rich AAIW is linked to the North Atlantic climate (Jung et al., 2009; Pahnke and Zahn, 2005). The maxima in the northward extension and, therefore, ventilation of the Arabian Sea water column are found during the Heinrich stadials. In contrast, minima extension occurred during interstadials with a stronger monsoon (Jung et al., 2009). In total, the interplay of these three mentioned factors, the bipolar seesaw structure of the northern and southern hemispheric climate but also the climate and oceanic patterns on regional scale (e.g. Lemieux-Dudon et al., 2010; Stocker and Johnsen, 2003), may lead to the feature that some of the D–O events, as well as some of the Heinrich events (H4), are not represented in the Gulf of Oman record. Further, stronger northwesterly and northeasterly winds during stadials (Leuschner and Sirocko, 2000) could have induced stronger deep winter mixing compared to present and, therefore, better ventilation (Lu et al., 2023; Reichart et al., 1998).

A striking feature of our Gulf of Oman δ^{15}N record is the prominent triple peak of strong water column deoxygenation from D–O event 3 to D–O event 5 (Fig. 6b). This is in contrast to other Arabian Sea records that do not show a prominent triple peak from D–O event 3 to D–O event 5 but from 5 to 7, with a broader D–O 8 event beforehand (Schulz et al., 1998). Interestingly, at the core site, suboxic to anoxic bottom water conditions occur during D–O 2, whereas the OMZ in the water column was not developed. We speculate that the inflow of oxygen-depleted RSW into the Gulf of Oman was still strong and/or that the maxima northward extension of the ventilating AAIW and/or ICW was further south, while denitrification processes were not as strong as during other pronounced D–O events. This is also the case for a record from the southern Somali upwelling area (Fig. 7d). However, along the Oman upwelling area (Altabet et al., 2002), a strong SW monsoon could have favoured upwelling-induced denitrification and therefore a strengthening of the OMZ in this region only, albeit not as strongly as during former D–O events.

In contrast to other parts of the Arabian Sea, the water column in the Gulf of Oman was well ventilated during the whole LGM, indicated by low δ^{15}N values (Fig. 7) and by high benthic foraminiferal diversity (Fig. 6). The northern and northeastern Arabian Sea experienced a stronger and/or longer NE monsoon season during the LGM (Pichevin et al., 2007; Suthhof et al., 2001). Thus, the stronger wind-induced mixing may have resulted in a better-ventilated OMZ compared to the interstadials. A recent study from the Oman upwelling area also suggests slightly increased oxygenation in the upper water column ($\sim$ 600–820 m) during the LGM compared to during the modern interstadial (Lu et al., 2023). Further, less lateral transport of nutrient- and oxygen-poor waters from the Oman upwelling due to weakened SW winds was supposed to mitigate denitrification in the northern and northeastern Arabian Sea (Suthhof et al., 2001). In addition, a northward expansion of the well-oxygenated AAIW during stadials results in better-ventilated intermediate waters in the Arabian Sea, reducing the strength of the OMZ (Jung et al., 2009; Pichevin et al., 2007). However, the productivity was still high enough to maintain an OMZ. The absence of the OMZ at the core location from the LGM to the beginning of the Bølling–Allerød (B–A) events may be due to more intense northwesterly winds in the Gulf of Oman and the NE monsoon (Leuschner and Sirocko, 2000; Sirocko et al., 2000) leading to stronger wind-induced mixing and ventilation of the water column. Weak Indian summer monsoon phases also occurred during the LGM in NE India (Dutt et al., 2015) and in the eastern Arabian Sea (Saravanan et al., 2020). In addition, Red Sea sea level was too low during that time (Sergiou et al., 2022; Siddall et al., 2003) to induce significant RSW influence on bottom water deoxygenation in the Gulf of Oman. The Persian Gulf plays no role in contributing water masses to the Gulf of Oman as it was nearly completely dry until the LGM and had no connection to the Gulf of Oman (Lambeck, 1996; Stoffers and Ross, 1979).

During the B–A interstadial, a strong OMZ and bottom water oxygenation occurred in the Gulf of Oman and was also observed for the whole Arabian Sea (Altabet et al., 2002; Ivanochko et al., 2005; Kessarkar et al., 2013; Orsi et al., 2017; Pichevin et al., 2007; Suthhof et al., 2001). Contrarily to the O_2 reconstruction of the benthic foraminifera, we see no distinct high ratios of (lycopane + n-C_{35})/n-C_{31} during the B–A interstadial. Here, it is possible that the threshold of oxygen depletion was not reached, preserving lycopane in the sediment.

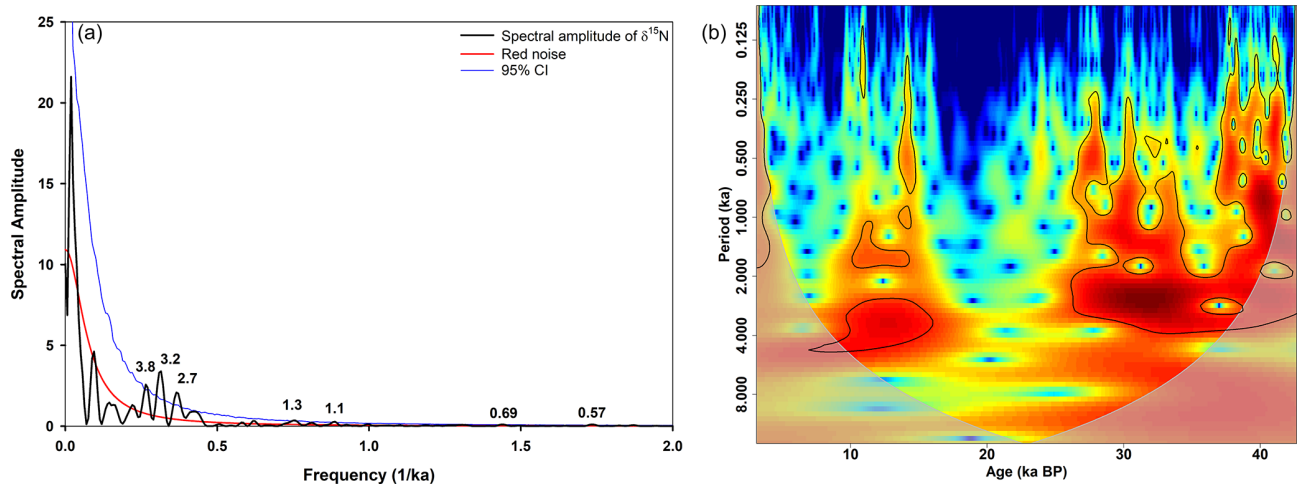

Figure 8. Spectral analysis **(a)** and wavelet power spectrum **(b)** of δ^{15}N of SL167. Red and blue lines in **(a)** indicate the red noise level and 95 % confidence interval (CI), respectively. Black numbers show significant periodicities on the 95 % CI. The black lines in **(b)** indicate the 95 % significance level. The colours in **(b)** represent the power of the wavelet power spectrum, with red (blue) showing high (low) power. The grey-shaded area represents the cone of influence.

5.1.2 Holocene

The observed low reconstructed O_2 contents and high δ^{15}N values with minor fluctuations during the Holocene indicate a continuously strong OMZ and sub-anoxic bottom water at the Oman margin area in the Gulf of Oman. This is in line with other studies for most parts of the Arabian Sea (Fig. 7, Altabet et al., 2002; Burdanowitz et al., 2019; Gaye et al., 2018; Kessarkar et al., 2013; Pichevin et al., 2007; Suthhof et al., 2001). In the course of the post-LGM sea level rise, the Persian Gulf became connected to the Gulf of Oman via the Strait of Hormuz at around 13 ka, with flooding of the central part of the Persian Gulf until about 11.5 ka (Lambeck, 1996). Since at least the mid-Holocene, the PGW has been an important factor in ventilating the upper OMZ (150–300 m) in the northern Arabian Sea (Lachkar et al., 2019). However, modern data show a relatively low increase in O_2 content (about 0.5 mol L^{-1}) due to PGW at (Fig. 1) and near the core location (Munz et al., 2017).

The highest ratios of (lycopane + n-C_{35})/n-C_{31} (> 1.0) occurred during the late Holocene, which may be due to relatively high total organic carbon mass accumulation rates during that time (Fig. A1) and thus is an effect of fast burial. This assumption is also corroborated by the increasing dominance of the opportunistic food indicator *Uvigerina peregrina* (Koho et al., 2008; Schmiedl et al., 2010), which favours a high supply of organic matter, leading to decreasing benthic foraminiferal diversity.

Overall, our multi-proxy oxygen record for the Gulf of Oman shows striking features. First, during most interstadial periods (D–O events and the Holocene) the denitrification and OMZ in the water column, as well as bottom water deoxygenation, were strong. Second, during MIS 3, oxygen conditions oscillated between moderately oxygenated (glacial) and deoxygenated or denitrification conditions (interglacial, D–O events), marking this period as an environmentally unstable period. Here, the oxygen concentrations were close to the threshold of suboxic and anoxic conditions and therefore fluctuated between oxia and suboxia, driven by changes in monsoon strength. In contrast, LGM or MIS 2 and the Holocene period show quite constant oxygen and deoxygenation and denitrification conditions, respectively. We argue that these two periods are stable enough to suppress strong oscillations of oxygenation versus deoxygenation.

5.2 Periodic changes and potential global drivers for OMZ strength and bottom water oxygenation

In order to identify specific periodicities, we have performed spectral and wavelet analyses for the δ^{15}N record (Fig. 8) and the oxygen (O_2) reconstruction of the benthic foraminifera (Fig. 9), respectively. For the strength of the OMZ in the water column based on δ^{15}N, we have found significant (95 % confidence interval, CI) periods of 3.8, 3.2, 2.7, 1.3 and 1.1 kyr, as well as 690 and 570 years (Fig. 8a). For the reconstructed O_2 bottom water variations, we have found significant periods (95 % CI) of 1.1 kyr and 710, 670, 600 and 570 years, as well as 3.2 kyr (90 % CI, Fig. 9a). These periods are mainly present between about 25–43 ka (MIS 3) and 8–16 ka (transition of LGM or MIS 2 to the Holocene, Figs. 8b and 9b) for both proxies. We attribute the periods of about 1.1–1.3 ka and around 3.2 ka to the D–O events as they occur within the periods of 1.5 and 3.0 ka approximately (Kuniyoshi et al., 2022; Schulz, 2002). In particular, the period of around 1.5 ka is a widespread feature in climate records (e.g. Bond et al., 2001; Jaglan et al., 2021; Lauterbach et al., 2014;

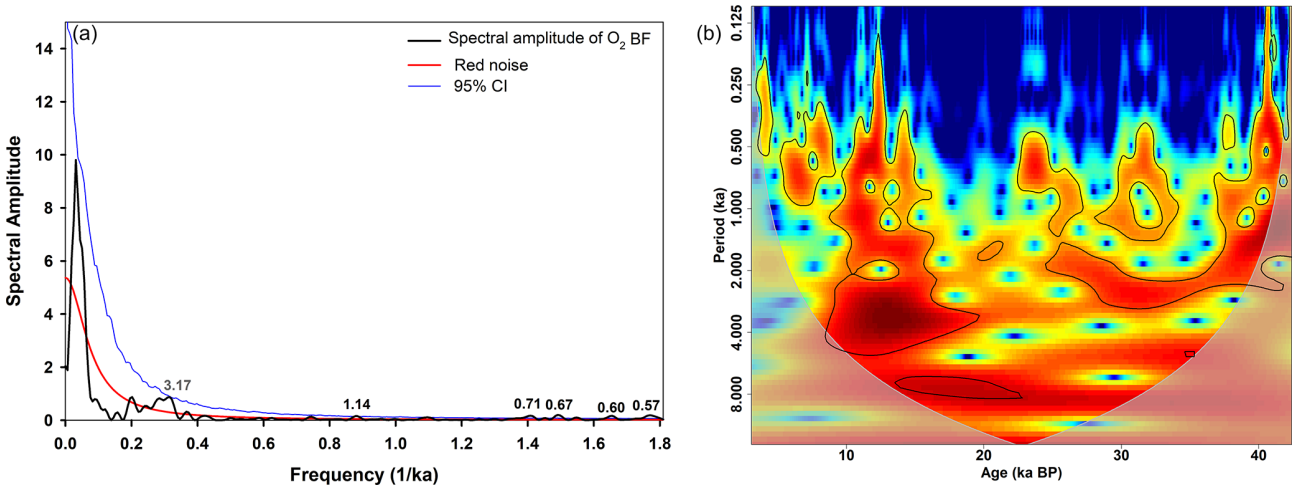

Figure 9. Spectral analysis **(a)** and wavelet power spectrum **(b)** of the reconstructed oxygen content of SL167 using benthic foraminifera assemblage (O_2 BF). Red and blue lines in **(a)** indicate the red noise level and 95 % confidence interval (CI), respectively. Black numbers show significant periodicities on the 95 % CI, and the grey number (3.17 ka) shows the significant periodicity at the 90 % CI. The black lines in **(b)** indicate the 95 % significance level. The colours in **(b)** represent the power of the wavelet power spectrum, with red (blue) showing high (low) power. The grey-shaded area represents the cone of influence.

Leuschner and Sirocko, 2000; Saravanan et al., 2020; Thamban et al., 2007; P. Wang et al., 2005). However, Obrochta et al. (2012) question the general idea of a 1.5 ka oscillation as they propose a superposition of the 1.0 and 2.0 ka cycles, which is also evident in our record with the 1.1 to 1.3 ka periods. Further strong evidence for D–O events as triggers of these periods is that the D–O events are also absent during the LGM or MIS 2 period (Buizert and Schmittner, 2015; North Greenland Ice Core Project members, 2004). The cold phase and its high global ice volume during the LGM inhibited an interstadial AMOC mode (strong AMOC and/or warm North Atlantic), which is required to initiate D–O events (Buizert and Schmittner, 2015). An interesting feature is the successive decrease in the duration and magnitude of the D–O events between two Heinrich events (Buizert and Schmittner, 2015). However, this pattern may or may not be the reason for the missing D–O 6 signal in our record as D–O 5 is strong and the last event between H4 and H3.

The periods of 570 to 710 years can be related to solar cycles (Liu et al., 2012; Stuiver and Braziunas, 1993; P. Wang et al., 2005). These cycles are prominent worldwide and are also found in the east Asian (Liu et al., 2012; Wang et al., 1999; P. Wang et al., 2005; Xu et al., 2014) and Indian monsoon (Burdanowitz et al., 2021; Neff et al., 2001; von Rad et al., 1999; Saravanan et al., 2020; Sarkar et al., 2000; Thamban et al., 2007) realms. Some authors attribute a 725–775-year periodicity to changes in the Indian summer monsoon (Saravanan et al., 2020) and in El Niño–Southern Oscillation (ENSO)-like cycles (Russell et al., 2003) or a harmonic cycle of the 1500-year cycle (von Rad et al., 1999), linked to the thermohaline circulation (Wang et al., 1999) or to the Intertropical Convergence Zone (ITCZ) movement in the tropics (Russell and Johnson, 2005). Most of the high-frequency periods (< 1000 years) are reported for the Holocene (Burdanowitz et al., 2021; Liu et al., 2012; Neff et al., 2001; von Rad et al., 1999; Russell et al., 2003; Russell and Johnson, 2005; Stuiver and Braziunas, 1993; Thamban et al., 2007; Wang et al., 1999; Y. Wang et al., 2005; Xu et al., 2014) or the LGM (Saravanan et al., 2020). Here, we show that these high-frequency periods are also present during MIS 3. The intensity and position of the monsoon system are driven by the summer insolation (precession signal) and the latitudinal temperature gradient (obliquity signal), respectively, with the latter being influenced by the latitudinal insolation gradient and ice cover (Davis and Brewer, 2009). The authors postulate that a strong latitudinal temperature gradient moves the monsoon system towards the Equator, which was the case during the LGM or MIS 2 for the summer (ca. 20–28 ka) and winter (ca. 18–25 ka) latitudinal temperature gradients (Davis and Brewer, 2009). This coincides with the well-ventilated water column and bottom water in the Gulf of Oman during that time, suggesting a response to the obliquity signal.

6 Conclusion

Our study presents a multi-proxy approach to reconstructing the water column and bottom water oxygenation in the Gulf of Oman for the past 43 kyr, approximately, for the first time. The three independent proxies based on bulk sediment ($\delta^{15}N$), lipid biomarker analysis (ratio of (lycopane + n-C_{35})/n-C_{31}) and benthic foraminifera taxa (enhanced benthic foraminiferal oxygen index, including transfer function of Kranner et al., 2022) show a robust and mostly consistent pat-

tern in our record. The Holocene is characterized by strong OMZ conditions and bottom water deoxygenation, which is consistent with other studies from the Arabian Sea. In contrast to other regions in the Arabian Sea, the water column and the bottom water in the Gulf of Oman were very well ventilated during the LGM or MIS 2. The well-oxygenated conditions of the Gulf of Oman lead to a highly diverse benthic foraminiferal assemblage. We attribute the good ventilation to stronger wind-induced mixing of the water column and better ventilation by oxygen-richer oceanic currents leading to stronger northward intrusion of the AAIW, corroborating other recent studies. The OMZ strength and bottom water oxygenation reconstruction during MIS 3 reveal oscillating conditions of moderately oxygenated (stadials) and deoxygenated conditions (interstadials, D–O events). Besides the prominent D–O cycles, we also found prominent high-frequency periods (570 to 710 years) during MIS 3 by using spectral and wavelet analyses.

In consideration of our results, we propose two different modes of the oxygenation status for the past 43 kyr, approximately. The first mode is a stable period of either strong OMZ and bottom water deoxygenation (Holocene) or a well-oxygenated water column and bottom water (MIS 2 including LGM). The second mode is an unstable period with oscillations between moderately oxygenated and deoxygenated conditions. This is visible in the MIS 3 period of our record with fluctuating high- and low-oxygen conditions.

Appendix A

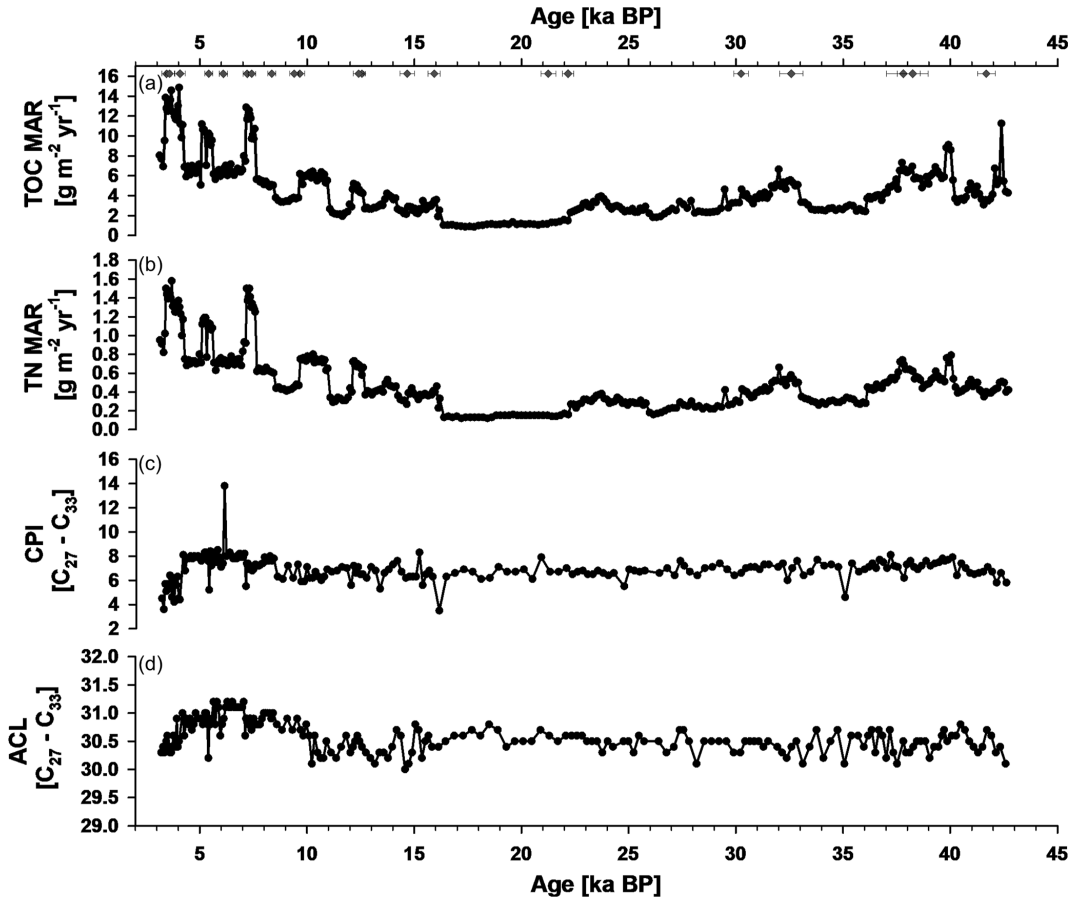

Figure A1. Bulk and plant-wax-derived *n*-alkane data of SL167. **(a)** Total mass accumulation rates of total organic carbon (TOC MAR), **(b)** total mass accumulation rates of total nitrogen (TN MAR), **(c)** carbon preference index (CPI) of the *n*-alkanes C_{27} to C_{33} and **(d)** average chain length (ACL) of the *n*-alkanes C_{27} to C_{33}. Diamonds show dated ages of SL167.

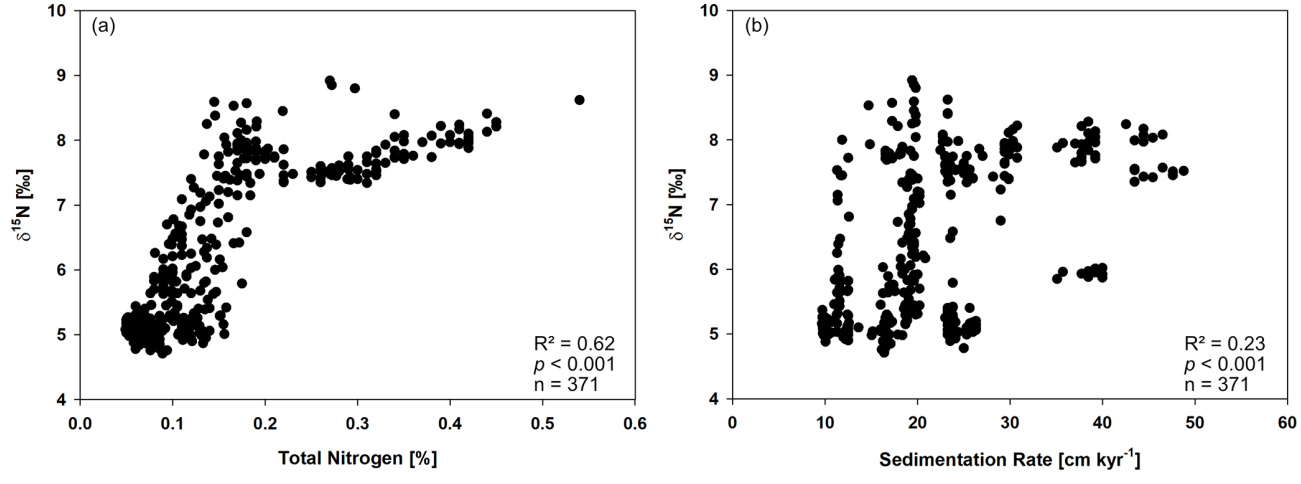

Figure A2. Cross plots of **(a)** total nitrogen (TN) and δ^{15}N, as well as **(b)** the sedimentation rate and δ^{15}N of sediment core SL167.

Data availability. The data sets are stored and available at PANGAEA under https://doi.org/10.1594/PANGAEA.964226 (Burdanowitz et al., 2024) and https://doi.org/10.1594/PANGAEA.960060 (Schmiedl et al., 2023b) (census date of benthic foraminifera).

Supplement. The supplement related to this article is available online at: https://doi.org/10.5194/bg-21-1477-2024-supplement.

Author contributions. NB: conceptualization, formal analysis, investigation, methodology, visualization, writing – original draft preparation. GS: conceptualization, faunal analysis, investigation, methodology, visualization, resources, supervision, writing – original draft preparation. BG: conceptualization, writing – original draft preparation. HS: faunal analysis, writing – original draft preparation. PM: faunal analysis, writing – original draft preparation.

Competing interests. The contact author has declared that none of the authors has any competing interests.

Disclaimer. Publisher's note: Copernicus Publications remains neutral with regard to jurisdictional claims made in the text, published maps, institutional affiliations, or any other geographical representation in this paper. While Copernicus Publications makes every effort to include appropriate place names, the final responsibility lies with the authors.

Acknowledgements. This work is funded by the Deutsche Forschungsgemeinschaft (DFG, German Research Foundation) under Germany's Excellence Strategy – EXC 2037 "CLICCS – Climate, Climatic Change, and Society" – project no. 390683824, a contribution to the Center for Earth System Research and Sustainability (CEN) of Universität Hamburg. Chlorophyll-*a* analyses and visualizations used in this paper were produced with the Giovanni online data system, developed and maintained by the NASA GES DISC. We also acknowledge the MODIS mission scientists and associated NASA personnel for the production of the data used in this research effort. We thank Frauke Langenberg, Marc Metzke, Miriam Warning, Jan Maier, Dorothea Bunzel, Tobias Winkler and Sabine Beckmann for the technical and analytical support. We also thank the two anonymous reviewers for their constructive comments and for improving the paper.

Financial support. This research has been supported by the Deutsche Forschungsgemeinschaft (grant no. 390683824).

Review statement. This paper was edited by Sebastian Naeher and reviewed by two anonymous referees.

References

Acharya, S. S. and Panigrahi, M. K.: Eastward shift and maintenance of Arabian Sea oxygen minimum zone: Understanding the paradox, Deep-Sea Res. Pt. I, 115, 240–252, https://doi.org/10.1016/j.dsr.2016.07.004, 2016.

Allard, J. L., Hughes, P. D., and Woodward, J. C.: Heinrich Stadial aridity forced Mediterranean-wide glacier retreat in the last cold stage, Nat. Geosci., 14, 197–205, https://doi.org/10.1038/s41561-021-00703-6, 2021.

Altabet, M. A., Francois, R., Murray, D. W., and Prell, W. L.: Climate-related variations in denitrification in the Arabian Sea from sediment $^{15}N/^{14}N$ ratios, Nature, 373, 506–509, https://doi.org/10.1038/373506a0, 1995.

Altabet, M. A., Pilskaln, C., Thunell, R., Pride, C., Sigman, D., Chavez, F., and Francois, R.: The nitrogen isotope biogeochemistry of sinking particles from the margin of the Eastern North Pacific, Deep-Sea Res. Pt. I, 46, 655–679, https://doi.org/10.1016/S0967-0637(98)00084-3, 1999.

Altabet, M. A., Higginson, M. J., and Murray, D. W.: The effect of millennial-scale changes in Arabian Sea denitrification on atmospheric CO_2, Nature, 415, 159–162, https://doi.org/10.1038/415159a, 2002.

Andruleit, H., Stäger, S., Rogalla, U., and Cepek, P.: Living coccolithophores in the northern Arabian Sea: Ecological tolerances and environmental control, Mar. Micropaleontol., 49, 157–181, https://doi.org/10.1016/S0377-8398(03)00049-5, 2003.

Arz, H. W., Lamy, F., Ganopolski, A., Nowaczyk, N., and Pätzold, J.: Dominant Northern Hemisphere climate control over millennial-scale glacial sea-level variability, Quaternary Sci. Rev., 26, 312–321, https://doi.org/10.1016/j.quascirev.2006.07.016, 2007.

Beal, L. M., Ffield, A., and Gordon, A. L.: Spreading of Red Sea overflow waters in the Indian Ocean, J. Geophys. Res.-Oceans, 105, 8549–8564, https://doi.org/10.1029/1999JC900306, 2000.

Blaauw, M. and Christen, J. A.: Flexible paleoclimate age-depth models using an autoregressive gamma process, Bayesian Anal., 6, 457–474, https://doi.org/10.1214/11-BA618, 2011.

Böll, A., Lückge, A., Munz, P., Forke, S., Schulz, H., Ramaswamy, V., Rixen, T., Gaye, B., and Emeis, K. C.: Late Holocene primary productivity and sea surface temperature variations in the northeastern Arabian Sea: Implications for winter monsoon variability, Paleoceanography, 29, 778–794, https://doi.org/10.1002/2013PA002579, 2014.

Bond, G., Kromer, B., Beer, J., Muscheler, R., Evans, M. N., Showers, W., Hoffmann, S., Lotti-Bond, R., Hajdas, I., and Bonani, G.: Persistent solar influence on North Atlantic climate during the Holocene, Science, 294, 2130–2136, https://doi.org/10.1126/science.1065680, 2001.

Bopp, L., Resplandy, L., Orr, J. C., Doney, S. C., Dunne, J. P., Gehlen, M., Halloran, P., Heinze, C., Ilyina, T., Séférian, R., Tjiputra, J., and Vichi, M.: Multiple stressors of ocean ecosystems in the 21st century: projections with CMIP5 models, Biogeosciences, 10, 6225–6245, https://doi.org/10.5194/bg-10-6225-2013, 2013.

Bower, A. S., Hunt, H. D., and Price, J. F.: Character and dynamics of the Red Sea and Persian Gulf outflows, J. Geophys. Res.-Oceans, 105, 6387–6414, https://doi.org/10.1029/1999JC900297, 2000.

Bray, E. . and Evans, E. .: Distribution of *n*-paraffins as a clue to recognition of source beds, Geochim. Cosmochim. Ac., 22, 2–15, https://doi.org/10.1016/0016-7037(61)90069-2, 1961.

Breitburg, D., Levin, L. A., Oschlies, A., Grégoire, M., Chavez, F. P., Conley, D. J., Garçon, V., Gilbert, D., Gutiérrez, D., Isensee, K., Jacinto, G. S., Limburg, K. E., Montes, I., Naqvi, S. W. A., Pitcher, G. C., Rabalais, N. N., Roman, M. R., Rose, K. A., Seibel, B. A., Telszewski, M., Yasuhara, M., and Zhang, J.: Declining oxygen in the global ocean and coastal waters, Science (80-.), 359, eaam7240, https://doi.org/10.1126/science.aam7240, 2018.

Bronough, D.: ncdf4.helpers: Helper Functions for Use with the "ncdf4" Package, R package version 0.3-6, CRAN [code], https://cran.r-project.org/package=ncdf4.helpers (last access: 8 August 2023), 2021.

Buizert, C. and Schmittner, A.: Southern Ocean control of glacial AMOC stability and Dansgaard–Oeschger interstadial duration, Paleoceanography, 30, 1595–1612, https://doi.org/10.1002/2015PA002795, 2015.

Bunn, A., Korpela, M., Biondi, F., Campelo, F., Mérian, P., Qeadan, F., and Zang, C.: dplR: Dendrochronology Program Library in R, R package version 1.7.4, CRAN [code], https://cran.r-project.org/package=dplR (last access: 27 June 2023), 2022.

Bunn, A. G.: A dendrochronology program library in R (dplR), Dendrochronologia, 26, 115–124, https://doi.org/10.1016/j.dendro.2008.01.002, 2008.

Bunn, A. G.: Statistical and visual crossdating in R using the dplR library, Dendrochronologia, 28, 251–258, https://doi.org/10.1016/j.dendro.2009.12.001, 2010.

Burdanowitz, N., Gaye, B., Hilbig, L., Lahajnar, N., Lückge, A., Rixen, T., and Emeis, K. C.: Holocene monsoon and sea level-related changes of sedimentation in the northeastern Arabian Sea, Deep. Res. Pt. II, 166, 6–18, https://doi.org/10.1016/j.dsr2.2019.03.003, 2019.

Burdanowitz, N., Rixen, T., Gaye, B., and Emeis, K.-C.: Signals of Holocene climate transition amplified by anthropogenic land-use changes in the westerly–Indian monsoon realm, Clim. Past, 17, 1735–1749, https://doi.org/10.5194/cp-17-1735-2021, 2021.

Burdanowitz, N., Schmiedl, G., Gaye, B., Munz, P., and Schulz, H.: Age model and geochemistry data of sediment core GeoTü SL167, PANGAEA [data set], https://doi.org/10.1594/PANGAEA.964226, 2024.

Busecke, J. J. M., Resplandy, L., Ditkovsky, S. J., and John, J. G.: Diverging Fates of the Pacific Ocean Oxygen Minimum Zone and Its Core in a Warming World, AGU Adv., 3, e2021AV000470, https://doi.org/10.1029/2021AV000470, 2022.

Bush, R. T. and McInerney, F. A.: Leaf wax n-alkane distributions in and across modern plants: Implications for paleoecology and chemotaxonomy, Geochim. Cosmochim. Ac., 117, 161–179, https://doi.org/10.1016/j.gca.2013.04.016, 2013.

Buzas, M. A. and Gibson, T. G.: Species Diversity: Benthonic Foraminifera in Western North Atlantic, Science (80-.), 163, 72–75, https://doi.org/10.1126/science.163.3862.72, 1969.

Carr, A. S., Boom, A., Grimes, H. L., Chase, B. M., Meadows, M. E., and Harris, A.: Leaf wax n-alkane distributions in arid zone South African flora: Environmental controls, chemotaxonomy and palaeoecological implications, Org. Geochem., 67, 72–84, https://doi.org/10.1016/j.orggeochem.2013.12.004, 2014.

Casciotti, K. L.: Nitrogen and Oxygen Isotopic Studies of the Marine Nitrogen Cycle, Annu. Rev. Mar. Sci., 8, 379–407, https://doi.org/10.1146/annurev-marine-010213-135052, 2016.

Clift, P. D. and Plumb, R. A.: The Asian Monsoon: Causes, History and Effects, Cambridge University Press, Cambridge, ISBN 9781107630192, 2008.

Collister, J. W., Rieley, G., Stern, B., Eglinton, G., and Fry, B.: Compound-specific δ 13C analyses of leaf lipids from plants with differing carbon dioxide metabolisms, Org. Geochem., 21, 619–627, https://doi.org/10.1016/0146-6380(94)90008-6, 1994.

Cooper, R. J., Pedentchouk, N., Hiscock, K. M., Disdle, P., Krueger, T., and Rawlins, B. G.: Apportioning sources of organic matter in streambed sediments: An integrated molecular and compound-specific stable isotope approach, Sci. Total Environ., 520, 187–197, https://doi.org/10.1016/j.scitotenv.2015.03.058, 2015.

Cranwell, P. A.: Extractable and bound lipid components in a freshwater sediment, Geochim. Cosmochim. Ac., 42, 1523–1532, https://doi.org/10.1016/0016-7037(78)90023-6, 1978.

Cranwell, P. A.: Diagenesis of free and bound lipids in terrestrial detritus deposited in a lacustrine sediment, Org. Geochem., 3, 79–89, http://www.sciencedirect.com/science/article/pii/0146638081900024 (last access: 20 January 2014), 1981.

Cullen, H. M., DeMenocal, P. B., Hemming, S., Hemming, G., Brown, F. H., Guilderson, T., and Sirocko, F.: Climate change and the collapse of the Akkadian empire: Evidence from the deep sea, Geology, 28, 379–382, https://doi.org/10.1130/0091-7613(2000)28<379:CCATCO>2.0.CO;2, 2000.

Davis, B. A. S. and Brewer, S.: Orbital forcing and role of the latitudinal insolation/temperature gradient, Clim. Dynam., 32, 143–165, https://doi.org/10.1007/s00382-008-0480-9, 2009.

de Marez, C., L'Hégaret, P., Morvan, M., and Carton, X.: On the 3D structure of eddies in the Arabian Sea, Deep-Sea Res. Pt. I, 150, 103057, https://doi.org/10.1016/j.dsr.2019.06.003, 2019.

Debenay, J.-P.: A Guide to 1,000 Foraminifera from Southwestern Pacific, New Caledonia, Publications Scientifiques du Muséum, Muséum national d'Histoire naturelle, Paris, 2012.

Den Dulk, M.: Benthic foraminiferal response to Late Quaternary variations in surface water productivity and oxygenation in the northern Arabian Sea, Geol. Ultraiectina, 188, 1–205, 2000.

Deplazes, G., Lückge, A., Peterson, L. C., Timmermann, A., Hamann, Y., Hughen, K. A., Röhl, U., Laj, C., Cane, M. A., Sigman, D. M., and Haug, G. H.: Links between tropical rainfall and North Atlantic climate during the last glacial period, Nat. Geosci., 6, 213–217, https://doi.org/10.1038/ngeo1712, 2013.

Deplazes, G., Lückge, A., Stuut, J. B. W., Pätzold, J., Kuhlmann, H., Husson, D., Fant, M., and Haug, G. H.: Weakening and strengthening of the Indian monsoon during Heinrich events and Dansgaard–Oeschger oscillations, Paleoceanography, 29, 99–114, https://doi.org/10.1002/2013PA002509, 2014.

Dummann, W., Steinig, S., Hofmann, P., Lenz, M., Kusch, S., Flögel, S., Herrle, J. O., Hallmann, C., Rethemeyer, J., Kasper, H. U., and Wagner, T.: Driving mechanisms of organic carbon burial in the Early Cretaceous South Atlantic Cape Basin (DSDP Site 361), Clim. Past, 17, 469–490, https://doi.org/10.5194/cp-17-469-2021, 2021.

Dutt, S., Gupta, A. K., Clemens, S. C., Cheng, H., Singh, R. K., Kathayat, G., and Edwards, R. L.: Abrupt changes in Indian summer monsoon strength during 33,800 to

5500 years B. P., Geophys. Res. Lett., 42, 5526–5532, https://doi.org/10.1002/2015GL064015, 2015.

Eglinton, G. and Hamilton, R.: Leaf epicuticular waxes, Science, 156, 1322–1335, 1967.

Eglinton, T. I. and Eglinton, G.: Molecular proxies for paleoclimatology, Earth Planet. Sc. Lett., 275, 1–16, https://doi.org/10.1016/j.epsl.2008.07.012, 2008.

Esri: ArcGIS Desktop: Release 10.8. Redlands, Environmental Systems Research Institute [software], https://www.esri.com/en-us/arcgis/products/arcgis-desktop/overview (last access: 8 May 2020), 2019.

Farrington, J. W., Davis, A. C., Sulanowski, J., McCaffrey, M. A., McCarthy, M., Clifford, C. H., Dickinson, P., and Volkman, J. K.: Biogeochemistry of lipids in surface sediments of the Peru Upwelling Area at 15° S, Org. Geochem., 13, 607–617, https://doi.org/10.1016/0146-6380(88)90080-0, 1988.

Fleitmann, D., Cheng, H., Badertscher, S., Edwards, R. L., Mudelsee, M., Göktürk, O. M., Fankhauser, A., Pickering, R., Raible, C. C., Matter, A., Kramers, J., and Tüysüz, O.: Timing and climatic impact of Greenland interstadials recorded in stalagmites from northern Turkey, Geophys. Res. Lett., 36, L19707, https://doi.org/10.1029/2009GL040050, 2009.

Fontanier, C., Jorissen, F. J., Licari, L., Alexandre, A., Anschutz, P., and Carbonel, P.: Live benthic foraminiferal faunas from the Bay of Biscay: faunal density, composition, and microhabitats, Deep-Sea Res. Pt. I, 49, 751–785, https://doi.org/10.1016/S0967-0637(01)00078-4, 2002.

Freeman, K. H., Wakeham, S. G., and Hayes, J. M.: Predictive isotopic biogeochemistry: Hydrocarbons from anoxic marine basins, Org. Geochem., 21, 629–644, https://doi.org/10.1016/0146-6380(94)90009-4, 1994.

Friederich, G. E., Ledesma, J., Ulloa, O., and Chavez, F. P.: Air–sea carbon dioxide fluxes in the coastal southeastern tropical Pacific, Prog. Oceanogr., 79, 156–166, https://doi.org/10.1016/j.pocean.2008.10.001, 2008.

Gaye, B., Böll, A., Segschneider, J., Burdanowitz, N., Emeis, K.-C., Ramaswamy, V., Lahajnar, N., Lückge, A., and Rixen, T.: Glacial–interglacial changes and Holocene variations in Arabian Sea denitrification, Biogeosciences, 15, 507–527, https://doi.org/10.5194/bg-15-507-2018, 2018.

Gaye-Haake, B., Lahajnar, N., Emeis, K. C., Unger, D., Rixen, T., Suthhof, A., Ramaswamy, V., Schulz, H., Paropkari, A. L., Guptha, M. V. S., and Ittekkot, V.: Stable nitrogen isotopic ratios of sinking particles and sediments from the northern Indian Ocean, Mar. Chem., 96, 243–255, https://doi.org/10.1016/j.marchem.2005.02.001, 2005.

GEBCO – General Bathymetric Chart of the Oceans: Gridded bathymetric data sets are global terrain models for ocean and land. A global 30 arc-second interval grid, The GEBCO_2014 Grid, version 20150318, BODC – British Oceanographic Data Centre, http://www.gebco.net (last access: 23 August 2021), 2014.

Gooday, A. J. B. T.: Benthic foraminifera (protista) as tools in deep-water palaeoceanography: Environmental influences on faunal characteristics, Adv. Mar. Biol., 46, 1–90, https://doi.org/10.1016/S0065-2881(03)46002-1, 2003.

Gouhier, T. C., Grinsted, A., and Simko, V.: R package biwavelet: Conduct Univariate and Bivariate Wavelet Analyses, R package version 0.20.21, CRAN [code], https://github.com/tgouhier/biwavelet (last access: 8 August 2023), 2021.

Gruber, N.: The Dynamics of the Marine Nitrogen Cycle and its Influence on Atmospheric CO_2 Variations, in: The Ocean Carbon Cycle and Climate, NATO Science Series, vol. 40, edited by: Follows, M. and Oguz, T., Springer Netherlands, Dordrecht, 97–148, https://doi.org/10.1007/978-1-4020-2087-2_4, 2004.

Haake, B., Ittekkot, V., Rixen, T., Ramaswamy, V., Nair, R. R., and Curry, W. B.: Seasonality and interannual variability of particle fluxes to the deep Arabian sea, Deep-Sea Res. Pt. I, 40, 1323–1344, https://doi.org/10.1016/0967-0637(93)90114-I, 1993.

Helly, J. J. and Levin, L. A.: Global distribution of naturally occurring marine hypoxia on continental margins, Deep-Sea Res. Pt. I, 51, 1159–1168, https://doi.org/10.1016/j.dsr.2004.03.009, 2004.

Herrmann, N., Boom, A., Carr, A. S., Chase, B. M., Granger, R., Hahn, A., Zabel, M., and Schefuß, E.: Sources, transport and deposition of terrestrial organic material: A case study from southwestern Africa, Quaternary Sci. Rev., 149, 215–229, https://doi.org/10.1016/j.quascirev.2016.07.028, 2016.

Hunt, K. M. R., Turner, A. G., and Shaffrey, L. C.: The evolution, seasonality and impacts of western disturbances, Q. J. Roy. Meteor. Soc., 144, 278–290, https://doi.org/10.1002/qj.3200, 2018.

Ivanochko, T. S., Ganeshram, R. S., Brummer, G.-J. A., Ganssen, G., Jung, S. J. A., Moreton, S. G., and Kroon, D.: Variations in tropical convection as an amplifier of global climate change at the millennial scale, Earth Planet. Sc. Lett., 235, 302–314, https://doi.org/10.1016/j.epsl.2005.04.002, 2005.

Jaglan, S., Gupta, A. K., Clemens, S. C., Dutt, S., Cheng, H., and Singh, R. K.: Abrupt Indian summer monsoon shifts aligned with Heinrich events and D-O cycles since MIS 3, Palaeogeogr. Palaeocl., 583, 110658, https://doi.org/10.1016/j.palaeo.2021.110658, 2021.

Jones, R. W.: The Challenger Foraminifera, Oxford University Press, Oxford, ISBN 0198540965, 1994.

Jorissen, F. J., de Stigter, H. C., and Widmark, J. G. V: A conceptual model explaining benthic foraminiferal microhabitats, Mar. Micropaleontol., 26, 3–15, https://doi.org/10.1016/0377-8398(95)00047-X, 1995.

Jung, M., Ilmberger, J., Mangini, A., and Emeis, K.-C.: Why some Mediterranean sapropels survived burn-down (and others did not), Mar. Geol., 141, 51–60, https://doi.org/10.1016/S0025-3227(97)00031-5, 1997.

Jung, S. J. A., Kroon, D., Ganssen, G., Peeters, F., and Ganeshram, R.: Enhanced Arabian Sea intermediate water flow during glacial North Atlantic cold phases, Earth Planet. Sc. Lett., 280, 220–228, https://doi.org/10.1016/j.epsl.2009.01.037, 2009.

Junium, C. K., Arthur, M. A., and Freeman, K. H.: Compound-specific $\delta^{15}N$ and chlorin preservation in surface sediments of the Peru Margin with implications for ancient bulk $\delta^{15}N$ records, Geochim. Cosmochim. Ac., 160, 306–318, https://doi.org/10.1016/j.gca.2014.12.018, 2015.

Kessarkar, P. M., Purnachadra Rao, V., Naqvi, S. W. A., and Karapurkar, S. G.: Variation in the Indian summer monsoon intensity during the Bølling-Ållerød and Holocene, Paleoceanography, 28, 413–425, https://doi.org/10.1002/palo.20040, 2013.

Koho, K. A., García, R., de Stigter, H. C., Epping, E., Koning, E., Kouwenhoven, T. J., and van der Zwaan, G. J.: Sedimentary labile organic carbon and pore water redox control on species distribution of benthic foraminifera: A case study from Lisbon–

Setúbal Canyon (southern Portugal), Prog. Oceanogr., 79, 55–82, https://doi.org/10.1016/j.pocean.2008.07.004, 2008.

Kranner, M., Harzhauser, M., Beer, C., Auer, G., and Piller, W. E.: Calculating dissolved marine oxygen values based on an enhanced Benthic Foraminifera Oxygen Index, Sci. Rep.-UK, 12, 1376, https://doi.org/10.1038/s41598-022-05295-8, 2022.

Kumar, S. P. and Prasad, T. G.: Formation and spreading of Arabian Sea high-salinity water mass, J. Geophys. Res.-Oceans, 104, 1455–1464, https://doi.org/10.1029/1998JC900022, 1999.

Kuniyoshi, Y., Abe-Ouchi, A., Sherriff-Tadano, S., Chan, W.-L., and Saito, F.: Effect of Climatic Precession on Dansgaard–Oeschger-Like Oscillations, Geophys. Res. Lett., 49, e2021GL095695, https://doi.org/10.1029/2021GL095695, 2022.

L'Hégaret, P., Duarte, R., Carton, X., Vic, C., Ciani, D., Baraille, R., and Corréard, S.: Mesoscale variability in the Arabian Sea from HYCOM model results and observations: impact on the Persian Gulf Water path, Ocean Sci., 11, 667–693, https://doi.org/10.5194/os-11-667-2015, 2015.

Lachkar, Z., Lévy, M., and Smith, K. S.: Strong Intensification of the Arabian Sea Oxygen Minimum Zone in Response to Arabian Gulf Warming, Geophys. Res. Lett., 46, 5420–5429, https://doi.org/10.1029/2018GL081631, 2019.

Lambeck, K.: Shoreline reconstructions for the Persian Gulf since the last glacial maximum, Earth Planet. Sc. Lett., 142, 43–57, https://doi.org/10.1016/0012-821x(96)00069-6, 1996.

Lauterbach, S., Witt, R., Plessen, B., Dulski, P., Prasad, S., Mingram, J., Gleixner, G., Hettler-Riedel, S., Stebich, M., Schnetger, B., Schwalb, A., and Schwarz, A.: Climatic imprint of the mid-latitude Westerlies in the Central Tian Shan of Kyrgyzstan and teleconnections to North Atlantic climate variability during the last 6000 years, Holocene, 24, 970–984, https://doi.org/10.1177/0959683614534741, 2014.

Lemieux-Dudon, B., Blayo, E., Petit, J.-R., Waelbroeck, C., Svensson, A., Ritz, C., Barnola, J.-M., Narcisi, B. M., and Parrenin, F.: Consistent dating for Antarctic and Greenland ice cores, Quaternary Sci. Rev., 29, 8–20, https://doi.org/10.1016/j.quascirev.2009.11.010, 2010.

Leuschner, D. C. and Sirocko, F.: The low-latitude monsoon climate during Dansgaard–Oeschger cycles and Heinrich Events, Quaternary Sci. Rev., 19, 243–254, https://doi.org/10.1016/S0277-3791(99)00064-5, 2000.

Levin, L. A.: Oxygen minimum zone Benthos: Adaptation and community response to hypoxia, Oceanogr. Mar. Biol., 41, 1–45, 2003.

Liu, H. Y., Lin, Z. S., Qi, X. Z., Li, Y. X., Yu, M. T., Yang, H., and Shen, J.: Possible link between Holocene East Asian monsoon and solar activity obtained from the EMD method, Nonlin. Processes Geophys., 19, 421–430, https://doi.org/10.5194/npg-19-421-2012, 2012.

Lu, W., Costa, K. M., and Oppo, D. W.: Reconstructing the Oxygen Depth Profile in the Arabian Sea During the Last Glacial Period, Paleoceanography and Paleoclimatology, 38, e2023PA004632, https://doi.org/10.1029/2023pa004632, 2023.

Madhupratap, M., Kumar, S. P., Bhattathiri, P. M. A., Kumar, M. D., Raghukumar, S., Nair, K. K. C., and Ramaiah, N.: Mechanism of the biological response to winter cooling in the northeastern Arabian Sea, Nature, 384, 549–552, https://doi.org/10.1038/384549a0, 1996.

Menzel, P., Gaye, B., Mishra, P. K., Anoop, A., Basavaiah, N., Marwan, N., Plessen, B., Prasad, S., Riedel, N., Stebich, M., and Wiesner, M. G.: Linking Holocene drying trends from Lonar Lake in monsoonal central India to North Atlantic cooling events, Palaeogeogr. Palaeocl., 410, 164–178, https://doi.org/10.1016/j.palaeo.2014.05.044, 2014.

Meyers, P. A. and Ishiwatari, R.: Lacustrine organic geochemistry—an overview of indicators of organic matter sources and diagenesis in lake sediments, Org. Geochem., 20, 867–900, https://doi.org/10.1016/0146-6380(93)90100-P, 1993.

Möbius, J., Gaye, B., Lahajnar, N., Bahlmann, E., and Emeis, K.-C.: Influence of diagenesis on sedimentary $\delta^{15}N$ in the Arabian Sea over the last 130 kyr, Mar. Geol., 284, 127–138, https://doi.org/10.1016/j.margeo.2011.03.013, 2011.

Montoya, J. P.: Nitrogen Stable Isotopes in Marine Environments, in: Nitrogen in the Marine Environment, edited by: Capone, D. G., Bronk, D. A., Mulholland, M. R., and Carpenter, E. J., Academic Press, San Diego, 1277–1302, https://doi.org/10.1016/B978-0-12-372522-6.00029-3, 2008.

Morrison, J. M., Codispoti, L. A., Gaurin, S., Jones, B., Manghnani, V., and Zheng, Z.: Seasonal variation of hydrographic and nutrient fields during the US JGOFS Arabian Sea Process Study, Deep-Sea Res. Pt. II, 45, 2053–2101, https://doi.org/10.1016/S0967-0645(98)00063-0, 1998.

Munz, P. M., Steinke, S., Böll, A., Lückge, A., Groeneveld, J., Kucera, M., and Schulz, H.: Decadal resolution record of Oman upwelling indicates solar forcing of the Indian summer monsoon (9–6 ka), Clim. Past, 13, 491–509, https://doi.org/10.5194/cp-13-491-2017, 2017.

Murray, J. W.: Ecology and palaeoecology of benthic foraminifera, Longman Scientific & Technical, New York, ISBN 9780582051225, 1991.

Naeher, S., Geraga, M., Papatheodorou, G., Ferentinos, G., Kaberi, H., and Schubert, C. J.: Environmental variations in a semi-enclosed embayment (Amvrakikos Gulf, Greece) – reconstructions based on benthic foraminifera abundance and lipid biomarker pattern, Biogeosciences, 9, 5081–5094, https://doi.org/10.5194/bg-9-5081-2012, 2012.

Naqvi, S. W. A., Bange, H. W., Farías, L., Monteiro, P. M. S., Scranton, M. I., and Zhang, J.: Marine hypoxia/anoxia as a source of CH_4 and N_2O, Biogeosciences, 7, 2159–2190, https://doi.org/10.5194/bg-7-2159-2010, 2010.

NASA: Moderate-resolution Imaging Spectroradiometer (MODIS) Aqua Chlorophyll Data, NASA OB.DAAC, Greenbelt, MD, USA, https://doi.org/10.5067/AQUA/MODIS/L3M/CHL/2022, 2022

Neff, U., Burns, S. J., Mangini, A., Mudelsee, M., Fleitmann, D., and Matter, A.: Strong coherence between solar variability and the monsoon in Oman between 9 and 6 kyr ago, Nature, 411, 290–293, https://doi.org/10.1038/35077048, 2001.

North Greenland Ice Core Project members: High-resolution record of Northern Hemisphere climate extending into the last interglacial period, Nature, 431, 147–151, https://doi.org/10.1038/nature02805, 2004.

Obrochta, S. P., Miyahara, H., Yokoyama, Y., and Crowley, T. J.: A re-examination of evidence for the North Atlantic " 1500-year cycle" at Site 609, Quaternary Sci. Rev., 55, 23–33, https://doi.org/10.1016/j.quascirev.2012.08.008, 2012.

Ogihara, S.: Is the lycopane/n-C31ratio an effective proxy of palaeoxicity of bottom water for the Japan Sea? – Unusual distribution of lycopane in the surface sediment from the Japan Sea collected by the MD179 cruise, J. Asian Earth Sci., 90, 250–253, https://doi.org/10.1016/j.jseaes.2013.12.012, 2014.

Orsi, W. D., Coolen, M. J. L., Wuchter, C., He, L., More, K. D., Irigoien, X., Chust, G., Johnson, C., Hemingway, J. D., Lee, M., Galy, V., and Giosan, L.: Climate oscillations reflected within the microbiome of Arabian Sea sediments, Sci. Rep.-UK, 7, 6040, https://doi.org/10.1038/s41598-017-05590-9, 2017.

Overpeck, J., Anderson, D., Trumbore, S., and Prell, W.: The southwest Indian Monsoon over the last 18000 years, Clim. Dynam., 12, 213–225, https://doi.org/10.1007/BF00211619, 1996.

Pahnke, K. and Zahn, R.: Southern Hemisphere Water Mass Conversion Linked with North Atlantic Climate Variability, Science (80-.), 307, 1741–1746, https://doi.org/10.1126/science.1102163, 2005.

Pancost, R. D. and Boot, C. S.: The palaeoclimatic utility of terrestrial biomarkers in marine sediments, Mar. Chem., 92, 239–261, https://doi.org/10.1016/j.marchem.2004.06.029, 2004.

Pathak, V. K., Kharwar, A., and Rai, A. K.: Benthic foraminiferal response to changes in the northwestern Arabian Sea oxygen minimum zone (OMZ) during past ∼ 145 kyr, J. Earth Syst. Sci., 130, 163, https://doi.org/10.1007/s12040-021-01659-2, 2021.

Paulmier, A. and Ruiz-Pino, D.: Oxygen minimum zones (OMZs) in the modern ocean, Prog. Oceanogr., 80, 113–128, https://doi.org/10.1016/j.pocean.2008.08.001, 2009.

Paulmier, A., Ruiz-Pino, D., and Garçon, V.: CO_2 maximum in the oxygen minimum zone (OMZ), Biogeosciences, 8, 239–252, https://doi.org/10.5194/bg-8-239-2011, 2011.

Pichevin, L., Bard, E., Martinez, P., and Billy, I.: Evidence of ventilation changes in the Arabian Sea during the late Quaternary: Implication for denitrification and nitrous oxide emission, Global Biogeochem. Cy., 21, GB4008, https://doi.org/10.1029/2006GB002852, 2007.

Pous, S. P., Carton, X., and Lazure, P.: Hydrology and circulation in the Strait of Hormuz and the Gulf of Oman—Results from the GOGP99 Experiment: 2. Gulf of Oman, J. Geophys. Res.-Oceans, 109, https://doi.org/10.1029/2003JC002146, 2004.

Prasad, T. G., Ikeda, M., and Kumar, S. P.: Seasonal spreading of the Persian Gulf Water mass in the Arabian Sea, J. Geophys. Res.-Oceans, 106, 17059–17071, https://doi.org/10.1029/2000JC000480, 2001.

R Core Team: R: A Language and Environment for Statistical Computing, R Foundation for Statistical Computing, Vienna, Austria, https://www.r-project.org/ (last access: 16 May 2023), 2023.

Reichart, G. J., den Dulk, M., Visser, H. J., van der Weijden, C. H., and Zachariasse, W. J.: A 225 kyr record of dust supply, paleoproductivity and the oxygen minimum zone from the Murray Ridge (northern Arabian Sea), Palaeogeogr. Palaeocl., 134, 149–169, https://doi.org/10.1016/S0031-0182(97)00071-0, 1997.

Reichart, G. J., Lourens, L. J., and Zachariasse, W. J.: Temporal variability in the northern Arabian Sea oxygen minimum zone (OMZ) during the last 225,000 years, Paleoceanography, 13, 607–621, https://doi.org/10.1029/98PA02203, 1998.

Reimer, P. J. and Reimer, R. W.: A Marine Reservoir Correction Database and On-Line Interface, Radiocarbon, 43, 461–463, https://doi.org/10.1017/S0033822200038339, 2001.

Rixen, T., Baum, A., Gaye, B., and Nagel, B.: Seasonal and interannual variations in the nitrogen cycle in the Arabian Sea, Biogeosciences, 11, 5733–5747, https://doi.org/10.5194/bg-11-5733-2014, 2014.

Rixen, T., Cowie, G., Gaye, B., Goes, J., do Rosário Gomes, H., Hood, R. R., Lachkar, Z., Schmidt, H., Segschneider, J., and Singh, A.: Reviews and syntheses: Present, past, and future of the oxygen minimum zone in the northern Indian Ocean, Biogeosciences, 17, 6051–6080, https://doi.org/10.5194/bg-17-6051-2020, 2020.

Rohling, E. J., Grant, K., Hemleben, C., Kucera, M., Roberts, A. P., Schmeltzer, I., Schulz, H., Siccha, M., Siddall, M., and Trommer, G.: New constraints on the timing of sea level fluctuations during early to middle marine isotope stage 3, Paleoceanography, 23, https://doi.org/10.1029/2008PA001617, 2008.

Rommerskirchen, F., Plader, A., Eglinton, G., Chikaraishi, Y., and Rullkötter, J.: Chemotaxonomic significance of distribution and stable carbon isotopic composition of long-chain alkanes and alkan-1-ols in C_4 grass waxes, Org. Geochem., 37, 1303–1332, https://doi.org/10.1016/j.orggeochem.2005.12.013, 2006.

Russell, J. M. and Johnson, T. C.: Late Holocene climate change in the North Atlantic and equatorial Africa: Millennial-scale ITCZ migration, Geophys. Res. Lett., 32, 1–4, https://doi.org/10.1029/2005GL023295, 2005.

Russell, J. M., Johnson, T. C., and Talbot, M. R.: A 725 yr cycle in the climate of central Africa during the late Holocene, Geology, 31, 677–680, https://doi.org/10.1130/G19449.1, 2003.

Sabino, M., Schefuß, E., Natalicchio, M., Dela Pierre, F., Birgel, D., Bortels, D., Schnetger, B., and Peckmann, J.: Climatic and hydrologic variability in the northern Mediterranean across the onset of the Messinian salinity crisis, Palaeogeogr. Palaeocl., 545, 109632, https://doi.org/10.1016/j.palaeo.2020.109632, 2020.

Sabino, M., Dela Pierre, F., Natalicchio, M., Birgel, D., Gier, S., and Peckmann, J.: The response of water column and sedimentary environments to the advent of the Messinian salinity crisis: insights from an onshore deep-water section (Govone, NW Italy), Geol. Mag., 158, 825–841, https://doi.org/10.1017/S0016756820000874, 2021.

Saravanan, P., Gupta, A. K., Zheng, H., Majumder, J., Panigrahi, M. K., and Kharya, A.: A 23000 year old record of paleoclimatic and environmental changes from the eastern Arabian Sea, Mar. Micropaleontol., 160, 101905, https://doi.org/10.1016/j.marmicro.2020.101905, 2020.

Sarkar, A., Ramesh, R., Somayajulu, B. L. K., Agnihotri, R., Jull, A. J. T., and Burr, O. S.: High resolution Holocene monsoon record from the eastern Arabian Sea, Earth Planet. Sc. Lett., 177, 209–218, https://doi.org/10.1016/S0012-821X(00)00053-4, 2000.

Schmidt, H., Czeschel, R., and Visbeck, M.: Seasonal variability of the Arabian Sea intermediate circulation and its impact on seasonal changes of the upper oxygen minimum zone, Ocean Sci., 16, 1459–1474, https://doi.org/10.5194/os-16-1459-2020, 2020.

Schmiedl, G., de Bovée, F., Buscail, R., Charrière, B., Hemleben, C., Medernach, L., and Picon, P.: Trophic control of benthic foraminiferal abundance and microhabitat in the bathyal Gulf of Lions, western Mediterranean Sea, Mar. Micropaleontol., 40, 167–188, https://doi.org/10.1016/S0377-8398(00)00038-4, 2000.

Schmiedl, G., Kuhnt, T., Ehrmann, W., Emeis, K.-C., Hamann, Y., Kotthoff, U., Dulski, P., and Pross, J.: Climatic forcing of east-

ern Mediterranean deep-water formation and benthic ecosystems during the past 22 000 years, Quaternary Sci. Rev., 29, 3006–3020, https://doi.org/10.1016/j.quascirev.2010.07.002, 2010.

Schmiedl, G., Milker, Y., and Mackensen, A.: Climate forcing of regional deep-sea biodiversity documented by benthic foraminifera, Earth-Sci. Rev., 244, 104540, https://doi.org/10.1016/j.earscirev.2023.104540, 2023a.

Schmiedl, G., Milker, Y., and Mackensen, A.: Benthic foraminifera census data of sediment core GeoTü SL167, PANGAEA [data set], https://doi.org/10.1594/PANGAEA.960060, 2023b.

Schott, F. A. and McCreary, J. P.: The monsoon circulation of the Indian Ocean, Prog. Oceanogr., 51, 1–123, https://doi.org/10.1016/S0079-6611(01)00083-0, 2001.

Schulte, S., Rostek, F., Bard, E., Rullkötter, J., and Marchal, O.: Variations of oxygen-minimum and primary productivity recorded in sediments of the Arabian Sea, Earth Planet. Sc. Lett., 173, 205–221, https://doi.org/10.1016/S0012-821X(99)00232-0, 1999.

Schulte, S., Mangelsdorf, K., and Rullkötter, J.: Organic matter preservation on the Pakistan continental margin as revealed by biomarker geochemistry, Org. Geochem., 31, 1005–1022, https://doi.org/10.1016/S0146-6380(00)00108-X, 2000.

Schulz, H., van Rad, U., and Erlenkeuser, H.: Correlation between Arabian Sea and Greenland climate oscillations of the past 110,000 years, Nature, 393, 54–57, https://doi.org/10.1038/31750, 1998.

Schulz, M.: On the 1470-year pacing of Dansgaard–Oeschger warm events, Paleoceanography, 17, 4–9, https://doi.org/10.1029/2000PA000571, 2002.

Schulz, M. and Mudelsee, M.: REDFIT: Estimating red-noise spectra directly from unevenly spaced paleoclimatic time series, Comput. Geosci., 28, 421–426, https://doi.org/10.1016/S0098-3004(01)00044-9, 2002.

Schumacher, S., Jorissen, F. J., Dissard, D., Larkin, K. E., and Gooday, A. J.: Live (Rose Bengal stained) and dead benthic foraminifera from the oxygen minimum zone of the Pakistan continental margin (Arabian Sea), Mar. Micropaleontol., 62, 45–73, https://doi.org/10.1016/j.marmicro.2006.07.004, 2007.

Sergiou, S., Geraga, M., Rohling, E. J., Rodríguez-Sanz, L., Hadjisolomou, E., Paraschos, F., Sakellariou, D., and Bailey, G.: Influences of sea level changes and the South Asian Monsoon on southern Red Sea oceanography over the last 30 ka, Quaternary Res., 110, 114–132, https://doi.org/10.1017/qua.2022.16, 2022.

Shenoi, S., Shetye, S. R., Gouveia, A. D., and Michael, G. S.: Salinity extrema in the Arabian Sea, Mitt. Geol.-Paläont. Inst. Univ. Hamburg, SCOPE/UNEP Sonderband, 76, 37–49, 1993.

Siddall, M., Rohling, E. J., Almogi-Labin, A., Hemleben, C., Meischner, D., Schmelzer, I., and Smeed, D. A.: Sea-level fluctuations during the last glacial cycle, Nature, 423, 853–858, https://doi.org/10.1038/nature01690, 2003.

Sigman, D. M. and Fripiat, F.: Nitrogen Isotopes in the Ocean, in: Encyclopedia of Ocean Sciences, 3rd Edn., edited by: Cochran, J. K., Bokuniewicz, H. J., and Yager, P. L., Academic Press, Oxford, 263–278, https://doi.org/10.1016/B978-0-12-409548-9.11605-7, 2019.

Sigman, D. M., Altabet, M. A., McCorkle, D. C., Francois, R., and Fischer, G.: The δ^{15}N of nitrate in the Southern Ocean: Nitrogen cycling and circulation in the ocean interior, J. Geophys. Res.-Oceans, 105, 19599–19614, https://doi.org/10.1029/2000JC000265, 2000.

Singh, A. D., Jung, S. J. A., Darling, K., Ganeshram, R., Ivanochko, T., and Kroon, D.: Productivity collapses in the Arabian Sea during glacial cold phases, Paleoceanography, 26, 1–10, https://doi.org/10.1029/2009PA001923, 2011.

Sinninghe Damsté, J. S., Kuypers, M. M. M., Schouten, S., Schulte, S., and Rullkötter, J.: The lycopane/C_{31} n-alkane ratio as a proxy to assess palaeoxicity during sediment deposition, Earth Planet. Sc. Lett., 209, 215–226, https://doi.org/10.1016/S0012-821X(03)00066-9, 2003.

Sirocko, F., Sarnthein, M., Lange, H., and Erlenkeuser, H.: Atmospheric summer circulation and coastal upwelling in the Arabian Sea during the Holocene and the last glaciation, Quaternary Res., 36, 72–93, https://doi.org/10.1016/0033-5894(91)90018-Z, 1991.

Sirocko, F., Garbe-Schönberg, Dieter and Devey, C.: Processes controlling trace element geochemistry of Arabian Sea sediments during the last 25,000 years, Global Planet. Change, 26, 217–303, https://doi.org/10.1016/S0921-8181(00)00046-1, 2000.

Southon, J., Kashgarian, M., Fontugne, M., Metivier, B., and W-S Yim, W.: Marine Reservoir Corrections for the Indian Ocean and Southeast Asia, Radiocarbon, 44, 167–180, https://doi.org/10.1017/S0033822200064778, 2002.

Staubwasser, M., Sirocko, F., Grootes, P. M., and Segl, M.: Climate change at the 4.2 ka BP termination of the Indus valley civilization and Holocene south Asian monsoon variability, Geophys. Res. Lett., 30, 1425, https://doi.org/10.1029/2002GL016822, 2003.

Steig, E. J., Jones, T. R., Schauer, A. J., Kahle, E. C., Morris, V. A., Vaughn, B. H., Davidge, L., and White, J. W. C.: Continuous-Flow Analysis of δ^{17}O, δ^{18}O, and δD of H_2O on an Ice Core from the South Pole, Front. Earth Sci., 9, 640292, https://doi.org/10.3389/feart.2021.640292, 2021.

Stocker, T. F. and Johnsen, S. J.: A minimum thermodynamic model for the bipolar seesaw, Paleoceanography, 18, 1087, https://doi.org/10.1029/2003PA000920, 2003.

Stoffers, P. and Ross, D. A.: Late Pleistocene and Holocene sedimentation in the Persian Gulf—Gulf of Oman, Sediment. Geol., 23, 181–208, https://doi.org/10.1016/0037-0738(79)90014-9, 1979.

Stuiver, M. and Braziunas, T. F.: Sun, ocean, climate and atmospheric 14CO2: an evaluation of causal and spectral relationships, Holocene, 3, 289–305, https://doi.org/10.1177/095968369300300401, 1993.

Suthhof, A., Ittekkot, V., and Gaye-Hakke, B.: Millennial-scale oscillation of denitrification intensity in the Arabian Sea during the late Quaternary and its potential influence on atmospheric N_20 and global climate, Global Biogeochem. Cy., 15, 637–649, 2001.

Szarek, R.: Biodiversity and biogeography of recent benthic foraminiferal assemblages in the south-western South China Sea (Sunda Shelf), University of Kiel, Kiel, Germany, https://nbn-resolving.org/urn:nbn:de:gbv:8-diss-5374 (last access: 15 January 2024), 2001.

Tesdal, J.-E., Galbraith, E. D., and Kienast, M.: Nitrogen isotopes in bulk marine sediment: linking seafloor observations with subseafloor records, Biogeosciences, 10, 101–118, https://doi.org/10.5194/bg-10-101-2013, 2013.

Thamban, M., Kawahata, H., and Rao, V. P.: Indian summer monsoon variability during the holocene as recorded in sediments of the Arabian Sea: Timing and implications, J. Oceanogr., 63, 1009–1020, https://doi.org/10.1007/s10872-007-0084-8, 2007.

Torrence, C. and Compo, G. P.: A practical guide to wavelet analysis, B. Am. Meteorol. Soc., 79, 61–78, 1998.

van Bentum, E. C., Hetzel, A., Brumsack, H.-J., Forster, A., Reichart, G.-J., and Sinninghe Damsté, J. S.: Reconstruction of water column anoxia in the equatorial Atlantic during the Cenomanian–Turonian oceanic anoxic event using biomarker and trace metal proxies, Palaeogeogr. Palaeocl., 280, 489–498, https://doi.org/10.1016/j.palaeo.2009.07.003, 2009.

Vogts, A., Moossen, H., Rommerskirchen, F., and Rullkötter, J.: Distribution patterns and stable carbon isotopic composition of alkanes and alkan-1-ols from plant waxes of African rain forest and savanna C3 species, Org. Geochem., 40, 1037–1054, https://doi.org/10.1016/j.orggeochem.2009.07.011, 2009.

von Rad, U., Schaaf, M., Michels, K. H., Schulz, H., Berger, W. H., and Sirocko, F.: A 5000-yr Record of Climate Change in Varved Sediments from the Oxygen Minimum Zone off Pakistan, Northeastern Arabian Sea, Quaternary Res., 51, 39–53, https://doi.org/10.1006/qres.1998.2016, 1999.

Wakeham, S. G.: Organic biogeochemistry in the oxygen-deficient ocean: A review, Org. Geochem., 149, 104096, https://doi.org/10.1016/j.orggeochem.2020.104096, 2020.

Wakeham, S. G., Freeman, K. H., Pease, T. K., and Hayes, J. M.: A photoautotrophic source for lycopane in marine water columns, Geochim. Cosmochim. Ac., 57, 159–165, https://doi.org/10.1016/0016-7037(93)90476-D, 1993.

Wang, L., Sarnthein, M., Erlenkeuser, H., Grimalt, J., Grootes, P., Heilig, S., Ivanova, E., Kienast, M., Pelejero, C., and Pflaumann, U.: East Asian monsoon climate during the Late Pleistocene: high-resolution sediment records from the South China Sea, Mar. Geol., 156, 245–284, https://doi.org/10.1016/S0025-3227(98)00182-0, 1999.

Wang, P., Clemens, S., Beaufort, L., Braconnot, P., Ganssen, G., Jian, Z., Kershaw, P., and Sarnthein, M.: Evolution and variability of the Asian monsoon system: State of the art and outstanding issues, Quaternary Sci. Rev., 24, 595–629, https://doi.org/10.1016/j.quascirev.2004.10.002, 2005.

Wang, Y., Cheng, H., Edwards, R. L., He, Y., Kong, X., An, Z., Wu, J., Kelly, M. J., Dykoski, C. A., and Li, X.: The Holocene Asian Monsoon: Links to Solar Changes and North Atlantic Climate, Science, 308, 854–857, https://doi.org/10.1126/science.1106296, 2005.

Wang, Y. J., Cheng, H., Edwards, R. L., An, Z. S., Wu, J. Y., Shen, C.-C., and Dorale, J. A.: A High-Resolution Absolute-Dated Late Pleistocene Monsoon Record from Hulu Cave, China, Science (80-.), 294, 2345–2348, https://doi.org/10.1126/science.1064618, 2001.

Wang, Z., DiMarco, S. F., Jochens, A. E., and Ingle, S.: High salinity events in the northern Arabian Sea and Sea of Oman, Deep-Sea Res. Pt. I, 74, 14–24, https://doi.org/10.1016/j.dsr.2012.12.004, 2013.

Xu, D., Lu, H., Chu, G., Wu, N., Shen, C., Wang, C., and Mao, L.: 500-year climate cycles stacking of recent centennial warming documented in an East Asian pollen record, Sci. Rep.-UK, 4, 3611, https://doi.org/10.1038/srep03611, 2014.

Zhou, Y., Gong, H., and Zhou, F.: Responses of Horizontally Expanding Oceanic Oxygen Minimum Zones to Climate Change Based on Observations, Geophys. Res. Lett., 49, e2022GL097724, https://doi.org/10.1029/2022GL097724, 2022.